

# SANDIA REPORT

SAND99-8206

Unlimited Release

Printed November 1998

## Homogeneous Charge Compression Ignition Free Piston Linear Alternator

Peter Van Blarigan, Scott Goldsborough, Nicholas Paradiso, Janson Wu

Prepared by  
Sandia National Laboratories  
Albuquerque, New Mexico 87185 and Livermore, California 94550

Sandia is a multiprogram laboratory operated by Sandia Corporation,  
a Lockheed Martin Company, for the United States Department of  
Energy under Contract DE-AC04-94AL85000.

Approved for public release; further dissemination unlimited.



**Sandia National Laboratories**

Issued by Sandia National Laboratories, operated for the United States Department of Energy by Sandia Corporation.

**NOTICE:** This report was prepared as an account of work sponsored by an agency of the United States Government. Neither the United States Government, nor any agency thereof, nor any of their employees, nor any of their contractors, subcontractors, or their employees, make any warranty, express or implied, or assume any legal liability or responsibility for the accuracy, completeness, or usefulness of any information, apparatus, product, or process disclosed, or represent that its use would not infringe privately owned rights. Reference herein to any specific commercial product, process, or service by trade name, trademark, manufacturer, or otherwise, does not necessarily constitute or imply its endorsement, recommendation, or favoring by the United States Government, any agency thereof, or any of their contractors or subcontractors. The views and opinions expressed herein do not necessarily state or reflect those of the United States Government, any agency thereof, or any of their contractors.

Printed in the United States of America. This report has been reproduced directly from the best available copy.

Available to DOE and DOE contractors from  
Office of Scientific and Technical Information  
P.O. Box 62  
Oak Ridge, TN 37831

Prices available from (615) 576-8401, FTS 626-8401

Available to the public from  
National Technical Information Service  
U.S. Department of Commerce  
5285 Port Royal Rd  
Springfield, VA 22161

NTIS price codes  
Printed copy: A04  
Microfiche copy: A01



# Homogeneous Charge Compression Ignition Free Piston Linear Alternator

Peter Van Blarigan, Scott Goldsborough, Nicholas Paradiso  
Engineering For Emerging Technology  
Janson Wu  
Exploratory Systems Technologies  
Sandia National Laboratories  
P.O. Box 969  
Livermore, CA 94551-0969, 9105

## Abstract

An experimental and theoretical investigation of a homogeneous charge compression ignition (HCCI) free piston powered linear alternator has been conducted to determine if improvements can be made in the thermal and conversion efficiencies of modern electrical generator systems. Performance of a free piston engine was investigated using a rapid compression expansion machine and a full cycle thermodynamic model. Linear alternator performance was investigated with a computer model. In addition linear alternator testing and permanent magnet characterization hardware were developed. The development of the two-stroke cycle scavenging process has begun.

Using a rapid compression expansion machine, the performance of ten different fuels was investigated at low equivalence ratio ( $\Phi \sim 0.35$ ) and initial temperatures of 25°C, 50°C and 70°C. The results indicate that by using high compression ratio ( $\sim 30:1$ ) and HCCI combustion the cycle indicated thermal efficiency can be significantly improved (56% measured) relative to conventional engines. The primary cause of this high conversion efficiency is nearly constant volume combustion. While low NO<sub>x</sub> emissions are possible (<10 PPM), HC and CO emissions must be controlled using an aftertreatment process.

Computer modeling of the linear alternator shows that a flux management system similar to that for a rotary alternator can be built without introducing any additional loss terms. In addition, the permanent magnet design can be utilized to start

the engine with the control accomplished by adjusting the impedance of the load on each coil.

## **Acknowledgement**

This work was supported by the U.S. Department of Energy, Office of Solar Thermal, Biomass Power and Hydrogen Technologies and the Laboratory Directed Research and Development program at Sandia National Laboratories. The authors gratefully acknowledge the technical assistance of David Zanini.

# Contents

Nomenclature .....	8
Introduction .....	9
Background .....	10
A New Combustion Approach .....	11
Engineering Configuration .....	13
Combustion Experiments .....	15
Experimental Results .....	17
Combustion Experiment Discussion .....	33
Linear Alternator .....	37
Fundamental Questions .....	37
Efficiency .....	38
Alternator Design .....	39
Starter Motor .....	40
Control System .....	41
Linear Alternator Testing .....	41
Free Piston Engine Model .....	43
Model Configuration .....	43
Model Results .....	43
Variations in Equivalence Ratio and Scavenging Efficiency ...	46
Control of the Scavenged Temperature .....	51
Compression Ratio Control .....	52
Model Discussion .....	54
Scavenging System .....	55
Scavenging Background .....	55
Design Approach .....	56
Conclusion .....	57
References .....	58

## Appendix

Rapid Compression Expansion Machine .....	61
---	----

## Figures

1 Free Piston Linear Alternator .....	13
2 Piston Position vs Time .....	15
3 Log Pressure vs Log Volume Extrapolation .....	16
4 Propane Log Pressure vs Log Volume .....	18
5 Pressure and Piston Position vs Time Near Top Dead Center ...	20
6 Propane Indicated Thermal Efficiency and NO <sub>x</sub> Emissions vs Compression Ratio .....	20

## Figures (continued)

7	Propane Unburned Hydrocarbon and Carbon Monoxide Emissions vs Compression Ratio .....	21
8	Natural Gas Log Pressure vs Log Volume .....	22
9	Natural Gas Indicated Thermal Efficiency and NO <sub>x</sub> Emissions vs Compression Ratio .....	23
10	Natural Gas Unburned Hydrocarbon and Carbon Monoxide Emissions vs Compression Ratio .....	23
11	Hydrogen Gas Log Pressure vs Log Volume .....	24
12	Hydrogen Indicated Thermal Efficiency and NO <sub>x</sub> Emissions vs Compression Ratio .....	24
13	Hydrogen Unburned Hydrocarbon and Carbon Monoxide Emissions vs Compression Ratio .....	25
14	Methanol Log Pressure vs Log Volume .....	26
15	Methanol Indicated Thermal Efficiency and NO <sub>x</sub> Emissions vs Compression Ratio .....	26
16	Methanol Unburned Hydrocarbon and Carbon Monoxide Emissions vs Compression Ratio .....	27
17	n-Pentane Log Pressure vs Log Volume .....	27
18	n-Pentane Two Stage Reaction Pressure vs Time .....	28
19	n-Pentane Indicated Thermal Efficiency and NO <sub>x</sub> Emissions vs Compression Ratio .....	29
20	n-Pentane Unburned Hydrocarbon and Carbon Monoxide Emissions vs Compression Ratio .....	29
21	Hexane Log Pressure vs Log Volume .....	30
22	Hexane Indicated Thermal Efficiency and NO <sub>x</sub> Emissions vs Compression Ratio .....	30
23	Hexane Unburned Hydrocarbon and Carbon Monoxide Emissions vs Compression Ratio .....	31
24	Heptane Log Pressure vs Log Volume .....	31
25	Heptane Indicated Thermal Efficiency and NO <sub>x</sub> Emissions vs Compression Ratio .....	32
26	Heptane Unburned Hydrocarbon and Carbon Monoxide Emissions vs Compression Ratio .....	32
27	Isooctane Log Pressure vs Log Volume .....	34
28	Isooctane Indicated Thermal Efficiency and NO <sub>x</sub> Emissions vs Compression Ratio .....	34
29	Isooctane Unburned Hydrocarbon and Carbon Monoxide Emissions vs Compression Ratio .....	35
30	Cutaway of Linear Alternator .....	37
31	Flux Generation Cutaway .....	39
32	Alternator Coil Circuit in Generator Mode .....	40
33	Linear Alternator Test Assembly .....	42
34	Piston Position vs Time .....	44
35	Piston Velocity vs Piston Position .....	44

## Figures (continued)

36 Pressure vs Time .....	45
37 Log Pressure vs Log Volume .....	45
38 Compression Ratio vs Equivalence Ratio .....	47
39 Compression Ratio vs Scavenging Efficiency .....	47
40 Compression Ratio vs Scavenged Temperature .....	48
41 Cycle Thermal Efficiency vs Compression Ratio .....	48
42 Overall Efficiency vs Compression Ratio .....	49
43 Oxide of Nitrogen Emissions vs Dilution Ratio Time .....	50
44 Cycle Thermal Efficiency, Overall Efficiency, and Short-Circuiting Ratio vs Scavenging Efficiency .....	51
45 Cycle Thermal Efficiency, Overall Efficiency, and Short-Circuiting Ratio vs Scavenging Efficiency .....	52
46 Cycle Thermal Efficiency vs Compression Ratio .....	53
47 Oxide of Nitrogen Emissions vs Compression Ratio .....	54

## Tables

1 Experimental Results .....	19
------------------------------	----

# Nomenclature

HCCI	homogeneous charge compression ignition
SI	spark ignition
IC	internal combustion
CR	compression ratio
RCEM	rapid compression expansion machine
RPM	revolutions per minute
TDC	top dead center
kW	kilowatt
IMEP	indicated mean effective pressure
CO	carbon monoxide exhaust emissions
HC	unburned hydrocarbon exhaust emissions
NO <sub>x</sub>	oxides of nitrogen exhaust emissions
NO	nitric oxide exhaust emissions
NO <sub>2</sub>	nitrogen dioxide exhaust emissions
N <sub>2</sub> O	nitrous oxide exhaust emissions
PPM	parts per million
EGR	exhaust gas recirculation
ATM	atmosphere
CARB	California Air Resources Board
SULEV	Super Ultra Low Emissions Vehicle
MGO	mega Gauss Osterands
RCEM	rapid compression expansion machine
$\Phi$	fuel/air equivalence ratio
T <sub>ini</sub>	initial temperature
$\eta_{th}$	indicated thermal efficiency

# Introduction

This report covers the work done to develop a homogeneous charge compression ignition (HCCI) free piston engine powered linear alternator. The goal in developing this generator set has been to maximize the thermal efficiency at a particular operating point while releasing essentially zero emissions. This approach should be applicable to both transportation and stationary power systems. The operating principle of the engine is to ignite and burn lean (fuel/air equivalence ratio ( $\Phi \sim 0.4$ ) homogeneous charge mixtures, while converting this energy release directly to electricity without the need for connecting rods or a crankshaft. Burning lean mixtures will improve the indicated thermal efficiency<sup>1</sup> while reducing the peak cylinder temperatures to a level where essentially no  $\text{NO}_x$  is formed<sup>2</sup>. It is projected that the California Air Resources Board's (CARB) proposed standard for super ultra low emissions vehicles (SULEV) will be met when the generator set is integrated into a series type hybrid power train for a standard size automobile<sup>2</sup>. (This projection is based on measured engine-out emissions from a conventional, but optimized for hydrogen, four stroke cycle spark ignition engine.)

The motivation for the present work derives from the fact that internal combustion (IC) engines used in series hybrid vehicle or stationary power system applications have operating requirements that are significantly different from IC engines used in conventional drivetrain applications. Shaft power is not required since all of the output power is converted directly to electrical energy with the engine cycling on and off as needed. In addition engine operation can be controlled automatically so that throttle response is unimportant.

In addition to operational differences, there are powerful incentives for advanced IC engines to have the capability of operating efficiently on a multitude of fuels (both conventional and unconventional) without significant hardware modification. Such versatile engines would help to improve the viability of fuels such as methanol and hydrogen.

The combination of these unique operating parameters and the results from our spark ignition engine program, has led us to formulate a new design specific to electric power applications, which is different from conventional configurations. The primary goals considered in this development are high energy conversion efficiencies and stringent emissions compliance. The result is an engine that operates on a unique homogeneous charge

compression ignition combustion process using a free piston geometry.

This report details the background behind the new concept, the experimental apparatus used to validate the combustion approach, the results of the combustion experiments, the linear alternator design and computer modeling, magnet testing, the full cycle thermodynamic modeling, a discussion of the scavenging design process, and the significance of the data obtained to date.

## Background

Fuel cells are generally considered to be ideal devices for advanced hybrid vehicles and stationary power systems where hydrogen or methane are used as fuels. In the near term however, the extensive development of the IC engine, and the existence of repair and maintenance industries associated with piston engines provide strong incentives to remain with this technology until fuel cells are proven reliable and cost competitive. In addition, while the fuel cell enjoys high public relations appeal, it seems possible that it may not offer significant efficiency advantages relative to an optimized combustion system. In light of these factors, the capabilities of internal combustion engines were reviewed. This is presented next.

In regards to thermodynamic efficiency, the Otto cycle theoretically represents the best option for an IC engine cycle. This is due to the fact that the fuel energy is converted to heat at constant volume when the working fluid is at maximum compression. This combustion condition leads to the highest possible peak temperatures, and thus the highest possible thermal efficiencies.

Edson<sup>3</sup> analytically investigated the efficiency potential of the ideal Otto cycle using compression ratios (CR) up to 300:1. The effects of chemical dissociation, working fluid thermodynamic properties, and chemical species concentration were included in his modeling. He found that even as the compression ratio is increased to 300:1, the thermal efficiency still increases for all of the fuels investigated. At this extreme operating point for instance, the cycle efficiency for isoctane fuel at stoichiometric ratio is over 80%.

Indeed it appears that no fundamental limit exists to achieving high efficiency from an internal combustion engine cycle.

However, many engineering challenges are involved in approaching ideal Otto cycle performance in real systems, especially where high compression ratios are utilized. Caris and Nelson<sup>4</sup> investigated the use of high compression ratios for improving the thermal efficiency of a production V8 spark ignition engine. They found that operation at compression ratios above about 17:1 did not continue to improve the thermal efficiency in their configuration. They concluded that this was due to the problem of non constant volume combustion, as time is required to propagate the spark ignited flame.

Other factors limiting the efficiency of IC engines include the transfer of heat energy from the combustion gases to the cylinder walls and the operating difficulties associated with increased pressure levels for engines configured to compression ratios above 25:1<sup>5,6</sup>. Still, finite burn duration remains the primary challenge to using high compression ratios.

The goal of emissions compliance further restricts the design possibilities for an optimized IC engine. For example, in order to eliminate the production of nitrogen oxides ( $\text{NO}_x$ ), the fuel/air mixture must be homogeneous and very lean at the time of combustion<sup>7,8</sup>. (It is subsequently possible to use oxidation catalyst technologies to sufficiently control other regulated emissions such as HC and CO.) Homogeneous operation precludes Diesel-type combustion, and spark ignition operation on premixed charges tends to limit the operating compression ratio due to uncontrolled autoignition, or knock. As well, very lean fuel/air mixtures are difficult, or impossible to spark ignite.

On the other hand, lean charges have more favorable specific heat ratios relative to stoichiometric mixtures, and this leads to improved cycle thermal efficiencies. Since three way catalysts are no longer required in this emissions controlling scheme the operating equivalence ratio does not need to be precisely controlled as it does in conventional stoichiometric operation. Equivalence ratio is defined here as the ratio of the actual fuel/air ratio to the stoichiometric ratio.

## **A New Combustion Approach**

Homogeneous charge compression ignition combustion can be used to solve the problems of burn duration and allow ideal Otto cycle operation to be more closely approached. In this combustion process a homogeneous charge of fuel and air is compression heated to the point of autoignition. Numerous ignition points

throughout the mixture can ensure very rapid combustion<sup>9</sup>. Very low equivalence ratios ( $\Phi \sim 0.3$ ) can be used since no flame propagation is required. Further, the useful compression ratio can be increased as higher temperatures are required to autoignite weak mixtures<sup>10</sup>.

HCCI operation is unconventional, but it is not new. As early as 1957 Alperstein, et al<sup>11</sup> experimented with premixed charges of hexane and air, and n-heptane and air in a Diesel engine. They found that under certain operating conditions their single cylinder engine would run quite well in a premixed mode with no fuel injection whatsoever.

In general, HCCI combustion has been shown to be faster than spark ignition or compression ignition combustion. And much leaner operation than in SI engines is possible, while lower NO<sub>x</sub> emissions result.

Most of the HCCI studies to date however, have concentrated on achieving smooth releases of energy under conventional compression conditions (CR ~ 9:1). Crankshaft driven pistons have been utilized in all of these previous investigations. Because of these operating parameters, successful HCCI operation has required extensive EGR and/or intake air preheating. Conventional pressure profiles have resulted<sup>12,13</sup>.

In order to maximize the efficiency potential of HCCI operation much higher compression ratios must be used, and a very rapid combustion event must be achieved. Recent work with higher compression ratios (~21:1) has demonstrated the high efficiency potential of the HCCI process<sup>14,15</sup>.

# Engineering Configuration

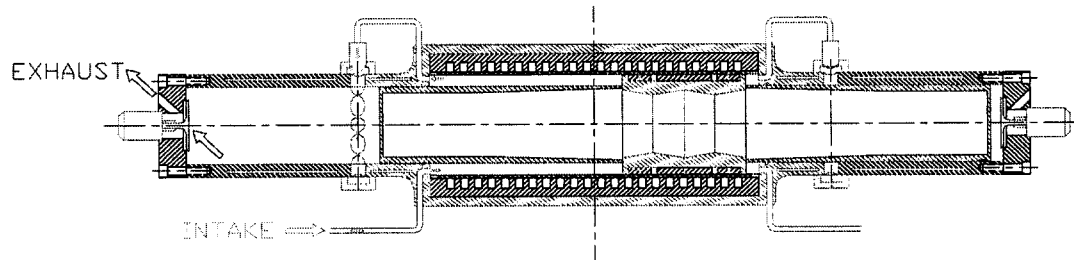


Figure 1 - Free piston linear alternator.

The free piston linear alternator illustrated in Figure 1 has been designed in hopes of approaching ideal Otto cycle performance through HCCI operation. In this configuration, high compression ratios can be used and rapid combustion can be achieved.

The linear generator is designed such that electricity is generated directly from the piston's oscillating motion, as permanent magnets fixed to the piston are driven back and forth through the alternator's coils. Combustion occurs alternately at each end of the piston and a modern two-stroke cycle scavenging process is used. The alternator component controls the piston's motion, and thus the extent of cylinder gas compression, by efficiently managing the piston's kinetic energy through each stroke. Compression of the fuel/air mixture is achieved inertially and as a result, a mechanically simple, variable compression ratio design is possible with sophisticated electronic control.

The use of free pistons in internal combustion engines has been investigated for quite some time. In the 1950's, experiments were conducted with free piston engines in automotive applications. In these early designs, the engine was used as a gasifier for a single stage turbine<sup>16,17</sup>. More recent developments have integrated hydraulic pumps into the engine's design<sup>18,19</sup>.

Several advantages have been noted for free piston IC engines. First, the compression ratio of the engine is variable, it is dependent mainly on the engine's operating conditions (e.g., fuel type, equivalence ratio, temperature, etc.). As a result, the desired compression ratio can be achieved through modification of the operating parameters, as opposed to changes in the engine's hardware.

An additional benefit is that the mechanical friction can be reduced relative to crankshaft driven geometries since there is only one moving engine part. Also, combustion seems to be faster than in conventional slider-crank configurations. Further, the unique piston dynamics (characteristically non-sinusoidal) seem to improve the engine's fuel economy and NO<sub>x</sub> emissions by limiting the time that the combustion gases spend at top dead center (TDC) (thereby reducing engine heat transfer and limiting the NO<sub>x</sub> kinetics). Finally, free piston engines are usually capable of operating on a variety of fuels.

The combination of the HCCI combustion process and the free piston geometry is expected to result in significant improvements in the engine's thermal efficiency and its exhaust emissions. The following advantages are predicted :

1. For a given maximum piston velocity, the free piston arrangement is capable of achieving a desired compression ratio more quickly than a crankshaft driven piston configuration. This point is illustrated in Figure 2 where the piston position profiles of both configurations are plotted.
2. The reduced compression time should result in higher compression of the premixed charge before the onset of autoignition.

High compression ratio operation is better suited to the free piston engine since the piston develops compression inertially, and as such there are no bearings or kinematic constraints that must survive high cylinder pressures or the high rates of pressure increase (shock). The use of low equivalence ratios in the HCCI application should further reduce the possibility of combustion chamber surface destruction<sup>20,21</sup>.

The free piston design is more capable of supporting low equivalence ratio operation and the correspondingly low IMEP levels due to the reduction in mechanical friction.

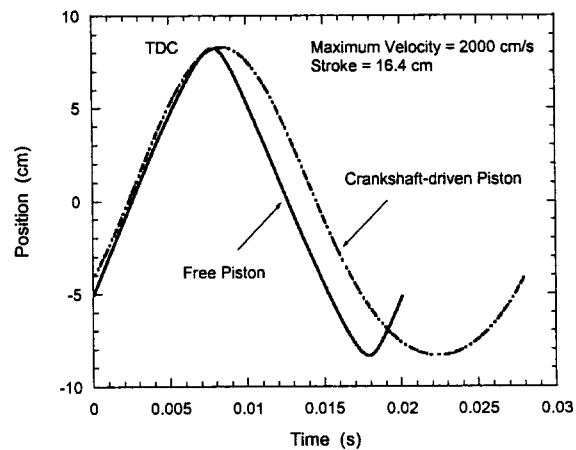


Figure 2 - Piston position vs. time.

## Combustion Experiments

While several new concepts are brought together in this generator design, it is the use of the free piston, HCCI combustion system that is the most significant. In order for the generator to be proven as a true advancement in IC engine technology, and to be able to compete with projected fuel cell capabilities, it is critical that the potential for high thermal efficiency and extremely low emissions be realized. To determine the achievable efficiencies and emissions reduction capabilities of the combustion system a series of experiments were conducted using a wide range of fuels.

A free piston rapid compression-expansion machine (RCEM) has been used for the initial testing. The RCEM consists of a double ended cylinder and a double ended free piston, where the enclosed piston is allowed to move freely along the cylinder's axis. In this device the combustion process is isolated from the rest of the engine cycle. The details of the RCEM and its operation can be found in the Appendix. A brief description of the combustion experiments is presented here.

Fuel/air mixtures of eight different fuels were tested using various initial temperatures where the energy density of the fuel/air charge was fixed. The eight fuels included propane, natural gas, hydrogen, methanol, n-pentane, hexane, n-heptane, and isooctane. The natural gas was composed of 93.13% methane,

3.2% ethane, 0.7% propane, 0.4% butane, 1.2% carbon dioxide, and 1.37% nitrogen by volume. An energy density of 1.15 kJ/L  $\pm$ 4% at STP was used for this study. (This was based on previous work with hydrogen in a modified spark ignition IC engine where the goal was to minimize the combustion temperatures, and thus the NO<sub>x</sub> emissions<sup>2</sup>.) The individual fuel/air equivalence ratios were adjusted to meet this energy value and are listed in Table 1. Initial charge temperatures of approximately 25°C, 50°C, and 70°C were used depending on the ease of autoigniting the mixture at the lower temperatures. For each testing condition a range of compression ratios was investigated, with these compression ratios adjusted depending on the fuel/air mixture's autoignition characteristics.

The metrics by which different experimental points are compared are the indicated thermal efficiency and the output emissions levels. The thermal efficiency was calculated by measuring both the pressure in the combustion chamber and the displacement of the piston. The net work was integrated over the compression and expansion strokes. Since the combusted gas is not fully expanded through the expansion stroke of the piston (as discussed in the Appendix), the full potential of the thermodynamic cycle was determined by extrapolating both the piston position and the cylinder pressure data. This was done by matching the expansion line slope on a logarithmic pressure - volume diagram, as shown in Figure 3.

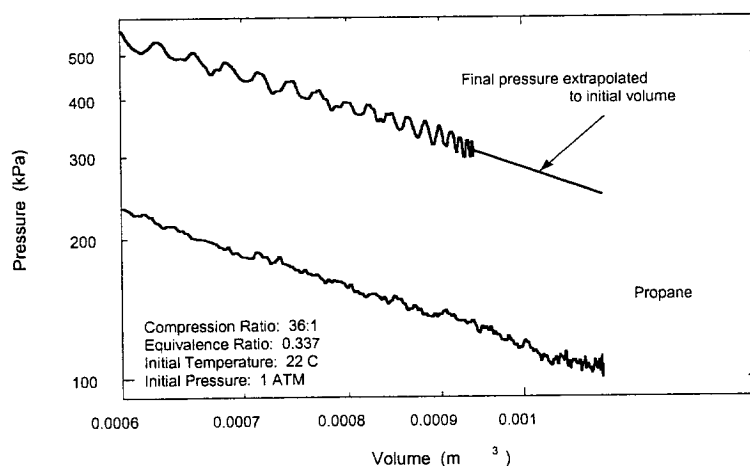


Figure 3 - Log pressure vs. log volume extrapolation

The NO<sub>x</sub>, HC, and CO concentrations of the combusted gases were measured using continuous exhaust gas emissions analyzers. Since only a small quantity of gas sample was available for each data point, modified measuring techniques were developed. These are also detailed in the Appendix.

3.2% ethane, 0.7% propane, 0.4% butane, 1.2% carbon dioxide, and 1.37% nitrogen by volume. An energy density of 1.15 kJ/L  $\pm$ 4% at STP was used for this study. (This was based on previous work with hydrogen in a modified spark ignition IC engine where the goal was to minimize the combustion temperatures, and thus the NO<sub>x</sub> emissions<sup>2</sup>.) The individual fuel/air equivalence ratios were adjusted to meet this energy value and are listed in Table 1. Initial charge temperatures of approximately 25°C, 50°C, and 70°C were used depending on the ease of autoigniting the mixture at the lower temperatures. For each testing condition a range of compression ratios was investigated, with these compression ratios adjusted depending on the fuel/air mixture's autoignition characteristics.

The metrics by which different experimental points are compared are the indicated thermal efficiency and the output emissions levels. The thermal efficiency was calculated by measuring both the pressure in the combustion chamber and the displacement of the piston. The net work was integrated over the compression and expansion strokes. Since the combusted gas is not fully expanded through the expansion stroke of the piston (as discussed in the Appendix), the full potential of the thermodynamic cycle was determined by extrapolating both the piston position and the cylinder pressure data. This was done by matching the expansion line slope on a logarithmic pressure - volume diagram, as shown in Figure 3.

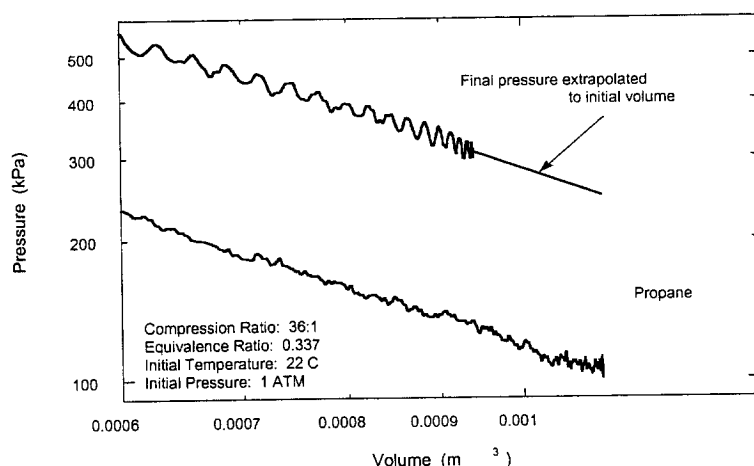


Figure 3 - Log pressure vs. log volume extrapolation

The NO<sub>x</sub>, HC, and CO concentrations of the combusted gases were measured using continuous exhaust gas emissions analyzers. Since only a small quantity of gas sample was available for each data point, modified measuring techniques were developed. These are also detailed in the Appendix.

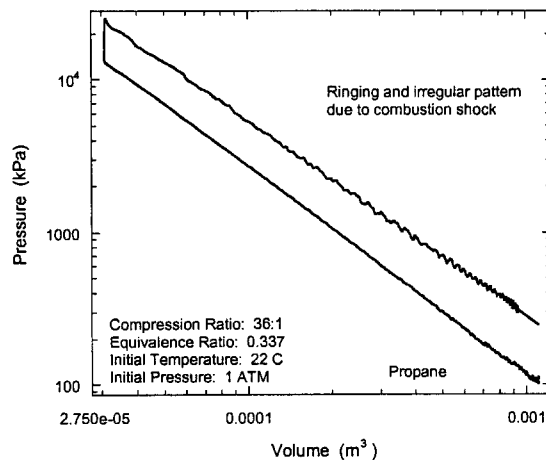


Figure 4 - Propane, log pressure vs. log volume.

In Figure 4 the similarity to the constant volume combustion process is evident. The rapidity of the HCCI process for this mixture is also illustrated in Figure 5 where the pressure vs. time curve is plotted. Autoignition occurs just at TDC and the duration of combustion is approximately 50  $\mu$ s. As can be seen, the piston has hardly moved during this time.

Noticeable in Figures 4 and 5 is the intensity of combustion. The burning event is so rapid that considerable ringing is generated in the pressure and displacement records (this accounts for the sawtooth pattern and other irregularities in the figures). The vibration of the experimental apparatus due to combustion is further discussed in detail in the Appendix.

Table 1 - Experimental Results.

Fuel	$\Phi$	$T_{ini}$ C	CR	$\eta_{th}$ %	$NO_x$ PPM	HC PPM	CO PPM
Dimethyl Ether	0.313	25	15-29	46-49	<10	280- 425	280- 1000
Ethanol	0.337	25,63	29-44	31-39	<20	525- 1350	500- 2500
n-Heptane	0.334	24	16-47	10-40	<5	2000- 4500	900- 3000
Hexane	0.336	26	19-34	40	<5	1000- 2000	1000- 2500
Hydrogen	0.319	22,49 67	17-50	40-55	1-550	<25	<120
Isooctane	0.321	25,70	16-74	30-55	1-70	800- 1050	300- 3000
Methanol	0.330	25	38-70	54-58	15-45	~600	300- 800
Natural Gas	0.365	23,67	30-54	50-55	10-130	600- 2000	250- 800
n-Pentane	0.335	25	23-36	47-50	<10	900- 1050	800- 1050
Propane	0.337	22,54	34-70	50-60	<15	100- 800	300- 800

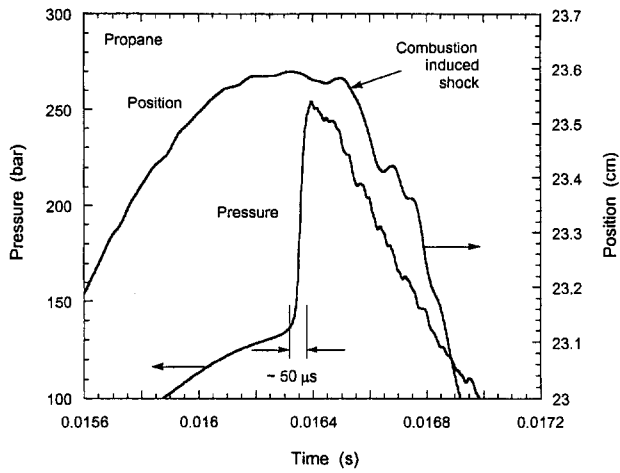


Figure 5 - Pressure and piston position vs. time near TDC.

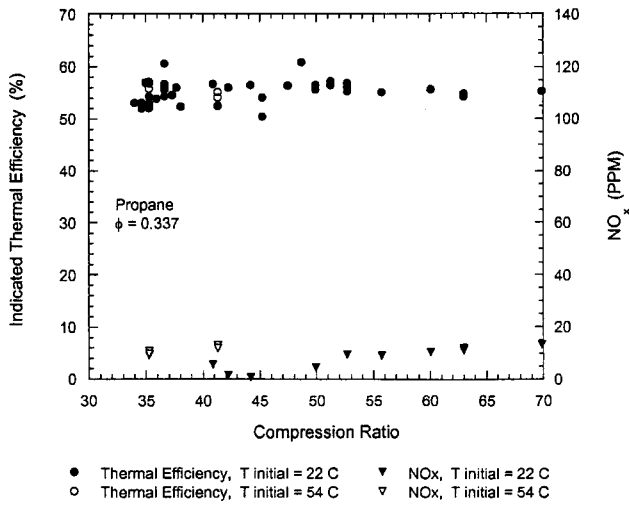


Figure 6 - Propane, indicated thermal efficiency and  $\text{NO}_x$  emissions vs. compression ratio.

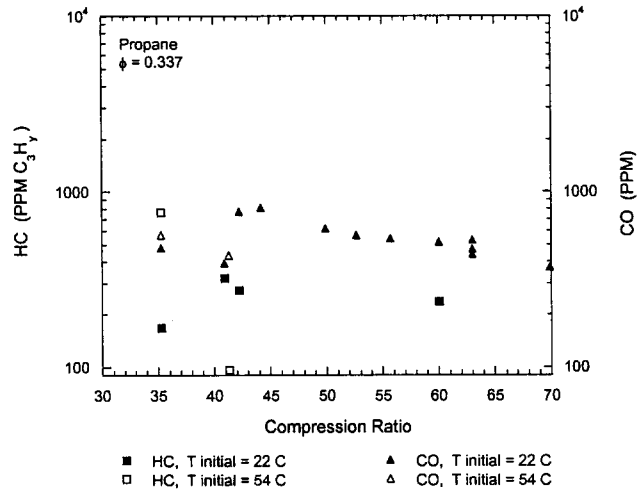


Figure 7 - Propane, HC and CO emissions vs. compression ratio.

Figure 6 gives the efficiency and  $\text{NO}_x$  levels as a function of compression ratio. Some of the  $\text{NO}_x$  emissions data are missing due to lost gas samples or the use of the combusted gases for analysis of gas leakage (as explained in the Appendix).

For an initial temperature of 22°C, autoignition of the propane/air mixture first occurs at a compression ratio of about 34:1. The calculated efficiencies are somewhat scattered but fairly steady after this point, falling between 50% and 60%. The tests performed using an initial temperature of 54°C are consistent with these results. The  $\text{NO}_x$  emissions levels are all below 15 PPM, increasing slightly with increased compression. The increase in  $\text{NO}_x$  was expected as the cylinder gases are compressed to higher temperatures after combustion.

Figure 7 plots the unburned hydrocarbon and carbon monoxide emissions as a function of compression ratio. Some of the HC and CO emissions data are also missing. Here the hydrocarbon emissions are reported as parts per million of  $\text{C}_3\text{H}_y$ .

With increasing compression there seems to be little pattern to the change in HC emissions, while the CO emissions tend to decrease with increased compression. The HC emissions range from 100 to 800 PPM, and the CO emissions vary from 300 to 800 PPM.

Figures 8, 9 and 10 give the log pressure vs. log volume, thermal efficiency and  $\text{NO}_x$  vs. compression ratio, and HC and CO emissions vs. compression ratio, respectively, for natural gas at an equivalence ratio of 0.365. Initial temperatures of 23°C and 67°C were used.

From Figure 8 it is evident that near constant volume combustion is possible with this fuel mixture. The duration of combustion in this case is approximately 65  $\mu$ s. This is slower than the propane/air mixture, but still relatively fast.

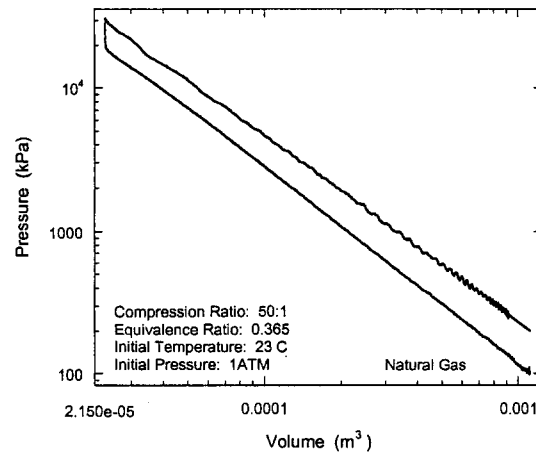


Figure 8 - Natural gas, log pressure vs. log volume.

The minimum compression ratio required for autoignition is much higher than that required for propane. At an initial temperature of 23°C late autoignition first occurs at about 44:1. At an initial temperature of 67°C the critical compression ratio is approximately 30:1. The thermal efficiency is fairly constant for both test conditions over the range of compression ratios investigated. There is less scatter in these points probably due to the refinement in the experimental procedure; typical results are about 54%. The NO<sub>x</sub> data show a more defined increasing trend with compression ratio, while the HC and CO emissions both decrease with compression ratio for each of the temperatures investigated.

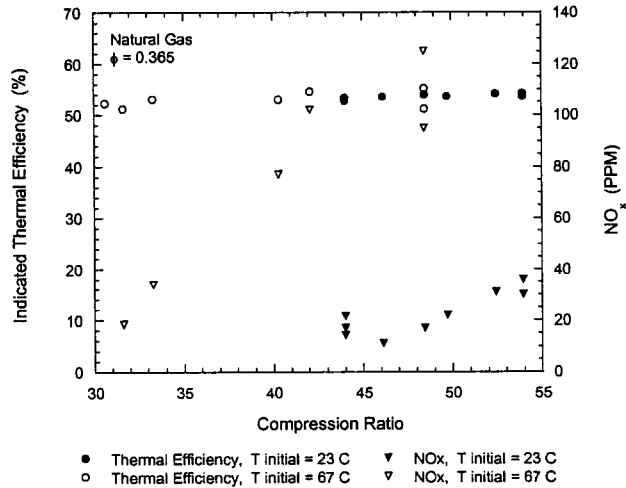


Figure 9 - Natural gas, indicated thermal efficiency and NO<sub>x</sub> emissions vs. compression ratio.

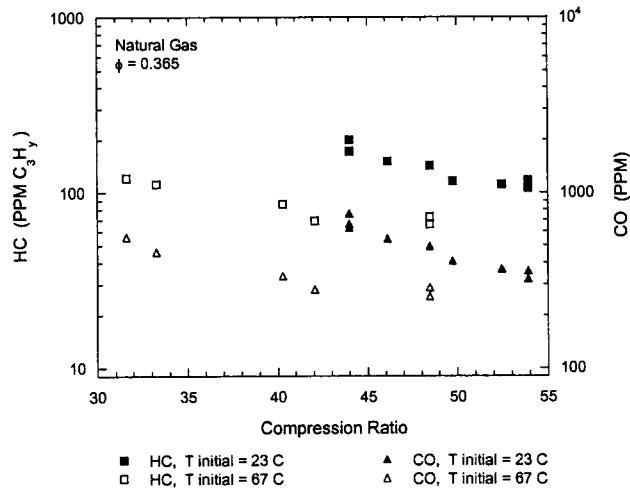


Figure 10 - Natural gas, HC and CO emissions vs. compression ratio.

Further oxidation of the cylinder gases seems to be the cause of the decrease in HC and CO emissions. Increased initial temperature only slightly affects the emissions levels.

It should be noted that the scales for the efficiency and emissions plots are the same as those for the propane/air mixture. It can be seen that the NO<sub>x</sub> and HC emissions for natural gas are higher than those for propane, however the CO emissions levels are comparable.

Figures 11, 12, and 13 show the results for hydrogen. In these runs an equivalence ratio of 0.319 was used at initial temperatures of 22°C, 49°C, and 67°C. Figure 11 illustrates the near constant volume combustion process for this fuel/air mixture at an initial temperature of 22°C. The duration of combustion is only 20  $\mu$ s, the shortest combustion time recorded for any of the fuels tested.

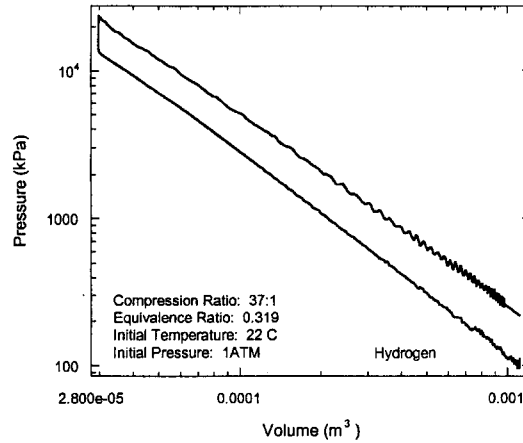


Figure 11 - Hydrogen, log pressure vs. log volume.

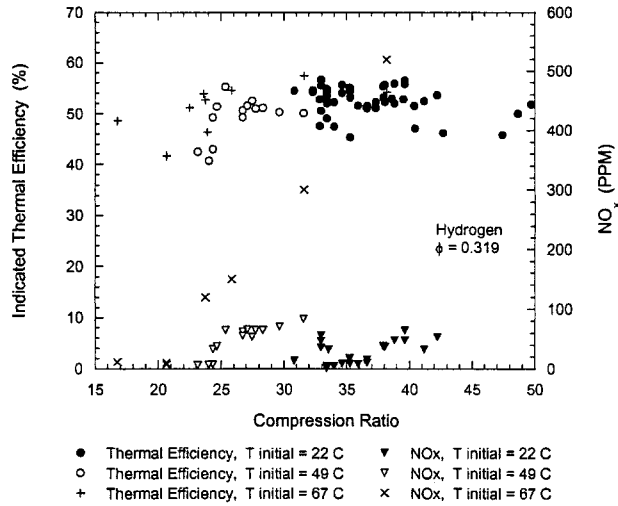


Figure 12 - Hydrogen, indicated thermal efficiency and NO<sub>x</sub> emissions vs. compression ratio.

The minimum compression ratios required for combustion are 30:1, 22:1, and 17:1 for initial temperatures of 22°C, 49°C, and 68°C, respectively. A significant amount of scatter is present in the

efficiency points due to the fact that hydrogen was the first fuel tested.

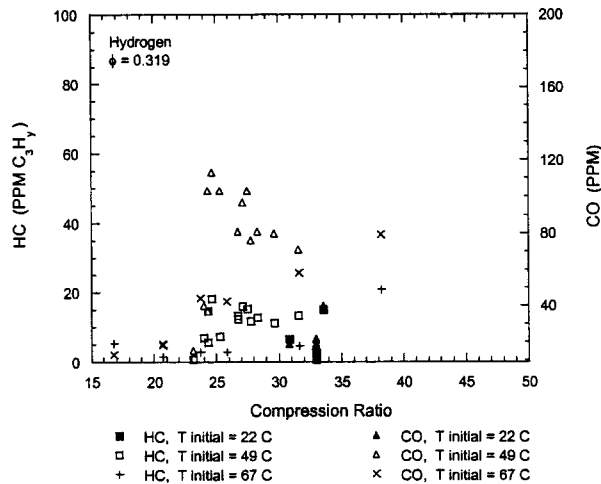


Figure 13 - Hydrogen, HC and CO emissions vs. compression ratio.

There seems to be little pattern to the change in efficiency with increased compression after TDC autoignition and only a small variation with changes in the starting temperature, even though the critical compression ratio is significantly affected.

The  $\text{NO}_x$  for hydrogen emissions are greater (a maximum of 530 PPM at an initial temperature of 67°C) than both the propane and natural gas mixtures, where the scale in Figure 12 is significantly increased. The  $\text{NO}_x$  levels for hydrogen also increase with compression of the cylinder charge after TDC combustion.

The HC and CO emissions data presented in Figure 13 represent the background emissions levels found in the system. These emissions are possibly due to contamination of the combustion chamber by piston ring lubricant oxidation, where this is discussed in the Appendix. (Ring lubricant oxidation could also be a source of error in the efficiency calculations for both hydrogen and propane fuels, where this would indicate higher than expected thermal efficiencies.) The hydrocarbon levels are below 20 PPM, and the carbon monoxide levels below 120 PPM.

The methanol test data is presented in Figures 14, 15 and 16. An equivalence ratio of 0.330 was used at an initial temperature of 25°C. From Figure 14, it is seen that near constant volume combustion is also possible with methanol. The duration of combustion is approximately 80 ms, and the critical compression ratio about 35:1.

The indicated efficiencies range from 54-58% with a slight increase with compression ratio. The  $\text{NO}_x$  emissions also increased slightly with compression, where the peak value was 43 PPM. The HC and CO emissions levels are comparable to the levels seen with propane, and the CO concentrations decrease with over-compression after TDC combustion.

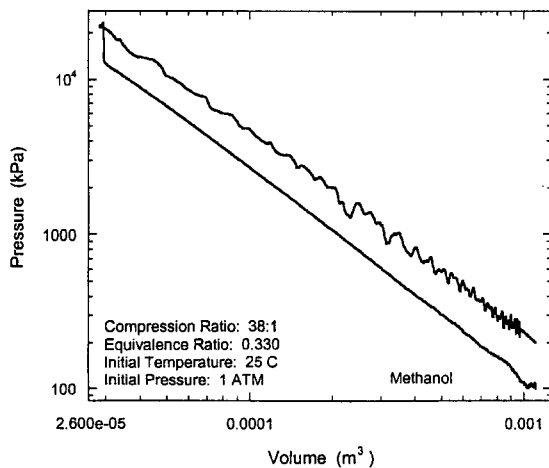


Figure 14 - Methanol, log pressure vs. log volume.

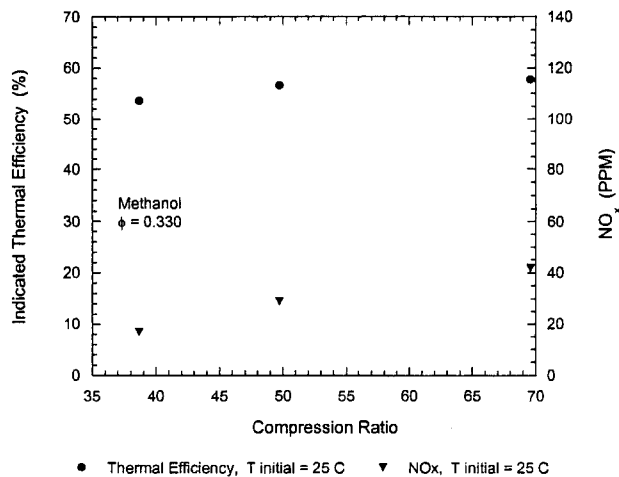


Figure 15 - Methanol, indicated thermal efficiency and  $\text{NO}_x$  emissions vs. compression ratio.

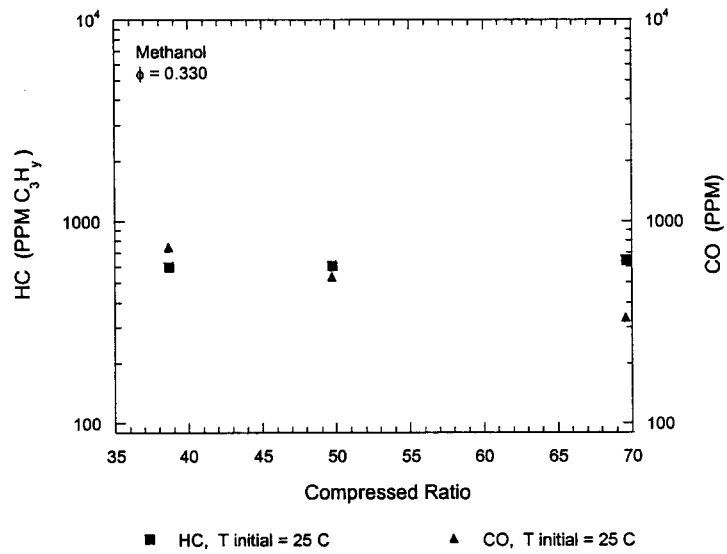


Figure 16 - Methanol, HC and CO emissions vs. compression ratio.

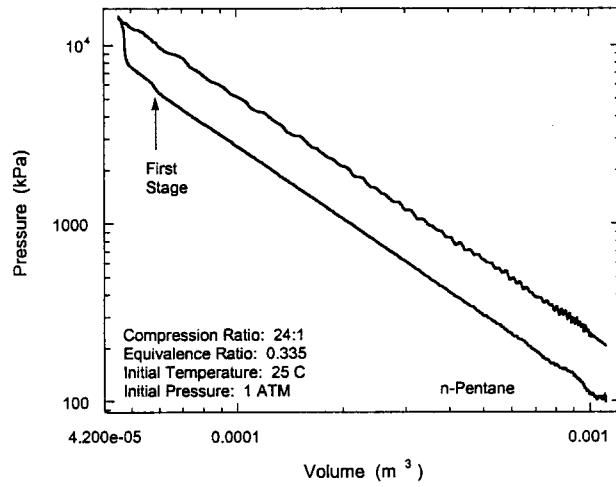


Figure 17 - n-Pentane, Log pressure vs. log volume.

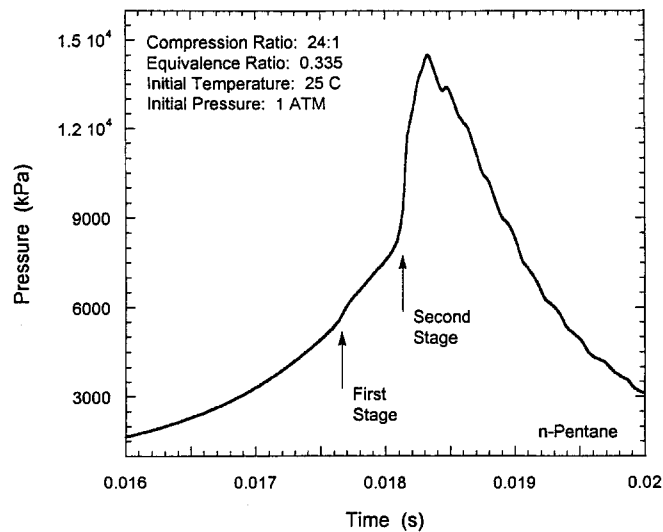


Figure 18 - n-Pentane, two stage reaction pressure vs. time.

The results from the n-pentane tests are presented in Figures 17-20. An equivalence ratio of 0.335 was used at an initial temperature of 25°C.

From Figure 17 it is evident that this fuel does not burn in a near constant volume process. Two stages of combustion are clearly discernable from this plot. The first stage of fuel decomposition occurs at a compression ratio of about 18:1, and further compression is required to more completely oxidize the fuel.

The second stage, or point of major heat release occurs at approximately 23:1. This two stage process is much slower than the HCCI processes previously seen, taking approximately 600 ms to complete.

The two stages of autoignition combustion are illustrated in Figure 18 where the pressure vs. time curve for this data point is plotted. The nature of this two stage HCCI process has been previously reported<sup>22</sup> where a rapid compression machine has been used to investigate the autoignition characteristics of various fuels.

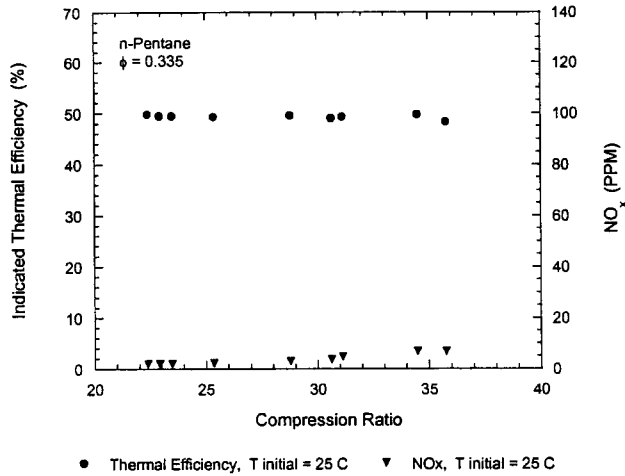


Figure 19 - n-Pentane, indicated thermal efficiency and NO<sub>x</sub> emissions vs. compression ratio.

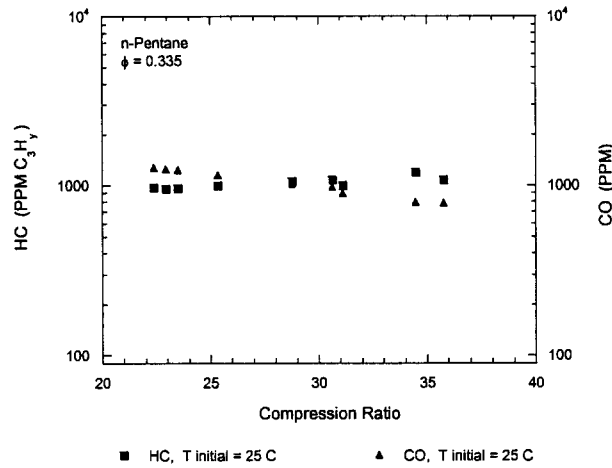


Figure 20 - n-Pentane, HC and CO emissions vs. compression ratio.

The efficiency calculations in Figure 19 exhibit a steady behavior with increasing compression, however, they are generally lower than the results from the previous fuels.

The NO<sub>x</sub> and HC emissions only slightly increase with compression and range from less than 10 PPM and 900-1050 PPM, respectively. The CO emissions decrease slightly with increasing compression ratio from about 1050 to 800 PPM. These concentrations are comparable to the other fuels.

The results for hexane are presented in Figures 21, 22, and 23. An equivalence ratio of 0.336 and an initial temperature of 25°C were used. Hexane also exhibited two-stage type HCCI combustion.

Again, near constant volume combustion was impossible, with the duration of combustion about 600  $\mu$ s.

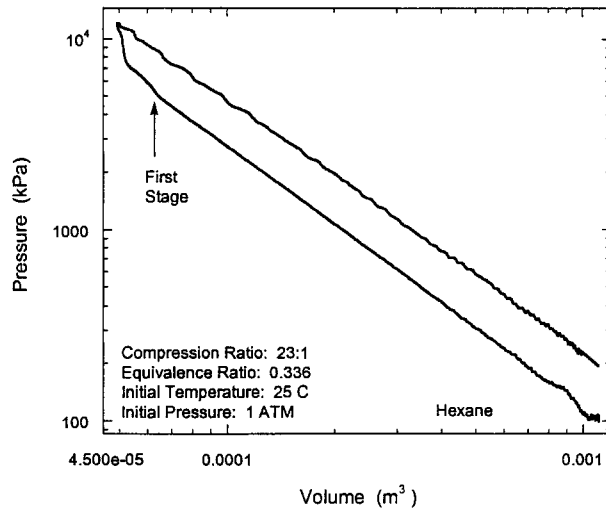


Figure 21 - Hexane, Log pressure vs. log volume.

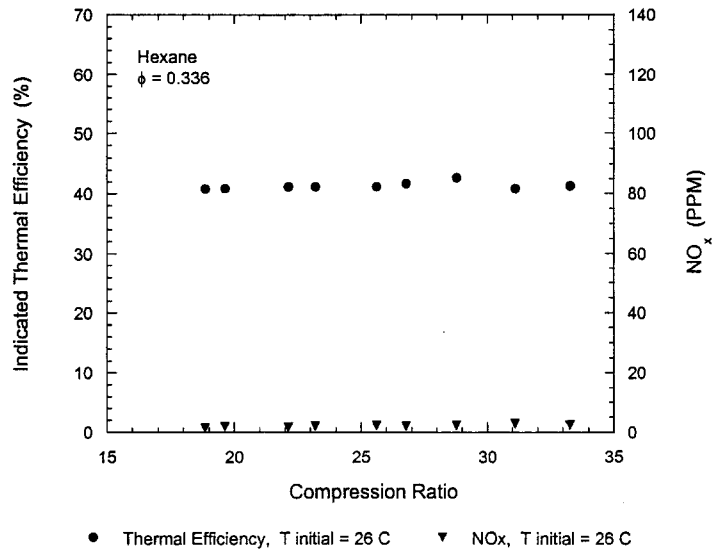


Figure 22 - Hexane, indicated thermal efficiency and  $\text{NO}_x$  emissions vs. compression ratio.

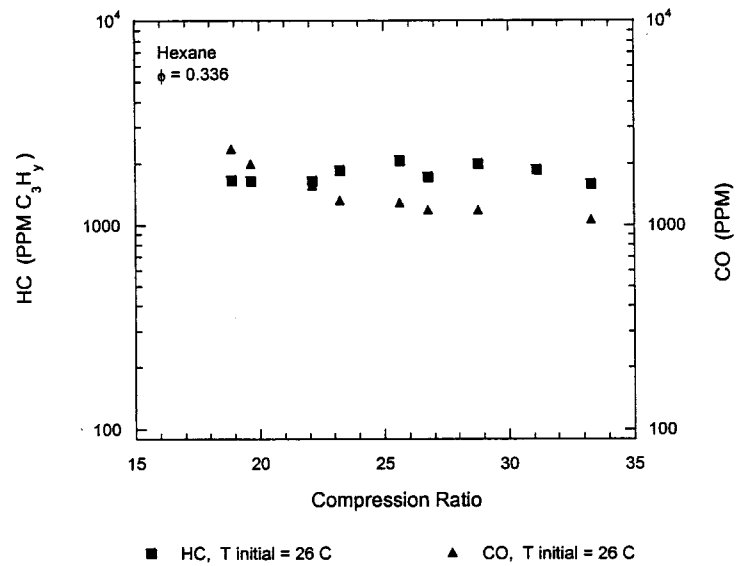


Figure 23 - Hexane, HC and CO emissions vs. compression ratio.

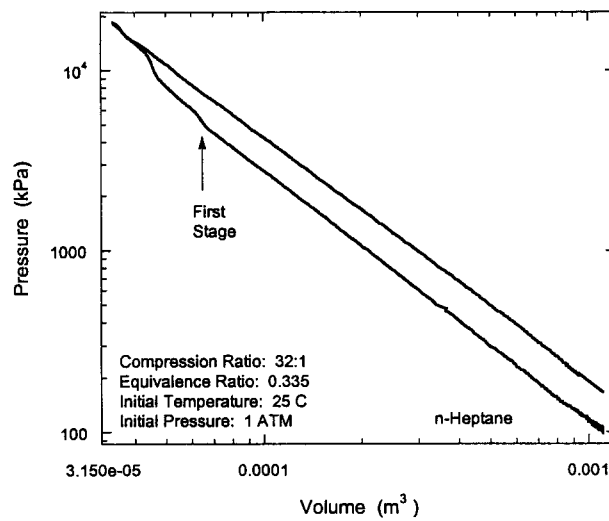


Figure 24 - Heptane, log pressure vs. log volume.

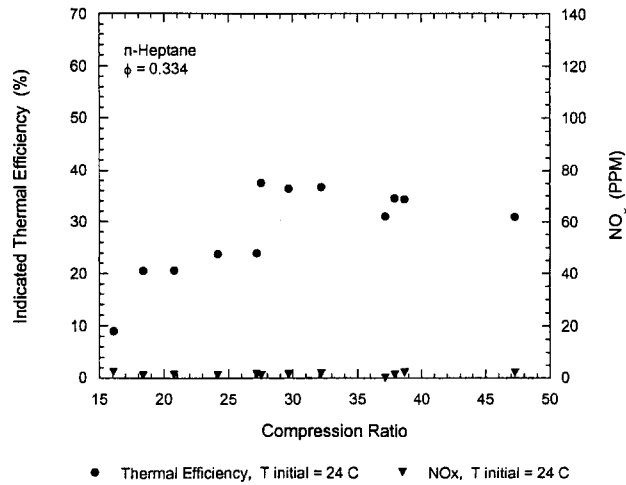


Figure 25 - Heptane, indicated thermal efficiency and NO<sub>x</sub> emissions vs. compression ratio.

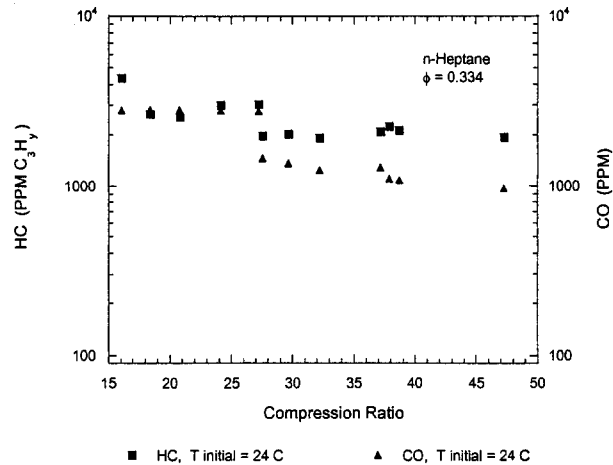


Figure 26 - Heptane, HC and CO emissions vs. compression ratio.

The efficiency and NO<sub>x</sub> and HC emissions for hexane are steady with compression ratio, while the CO emissions decrease. However, the results indicate that the HCCI process did not completely oxidize the fuel. The efficiency and NO<sub>x</sub> are low (40% and <5 PPM, respectively), while the HC and CO emissions are high (1000-3000 PPM) with respect to the other fuels.

Figures 24, 25, and 26 show the results for n-heptane. An equivalence ratio of 0.334 and an initial temperature of 24°C

were used. It is evident that the HCCI combustion process for n-heptane also proceeds in two stages.

The efficiency results from Figure 25 indicate that at low compression ratios some reaction of the fuel occurs, but even at compression ratios near 50:1 it does not appear that combustion goes to completion. The emissions data further support this conclusion. An increased initial temperature may improve the combustion conditions, however, this was not investigated.

The final data set is for isooctane, shown in Figures 27, 28 and 29. An equivalence ratio of 0.321 was used at initial temperatures of 25 and 70°C. Isooctane, like propane and natural gas, burned in a single step process and at nearly constant volume, as can be seen in Figure 27. However, the efficiency and emissions data indicate that the combustion process did not go to completion when the initial temperature was 25°C.

Further testing at 70°C seemed to improve the combustion conditions where higher efficiencies and lower emissions resulted. The trends with compression ratio at this starting temperature are similar to natural gas, however, the thermal efficiency is still lower than the most efficient fuels.

## Combustion Experiment Discussion

The purpose of the combustion experiments was to establish the potential for high efficiency and low emissions of the free piston, HCCI combustion process. The data presented here do illustrate that significant improvements relative to conventional technologies are possible.

Compared to ideal Otto cycles operating at standard compression ratios (12:1) and using stoichiometric mixtures (about the limit of today's SI engines with three-way catalysts), ideal Otto cycles operating on much higher compression ratios (30:1) and utilizing lean mixtures are capable of thermal efficiency improvements of near 40%. Our experiments show a similar improvement relative to contemporary engine performance<sup>6</sup> with fuels such as propane, hydrogen, and natural gas, where indicated efficiencies near 56% have been measured.

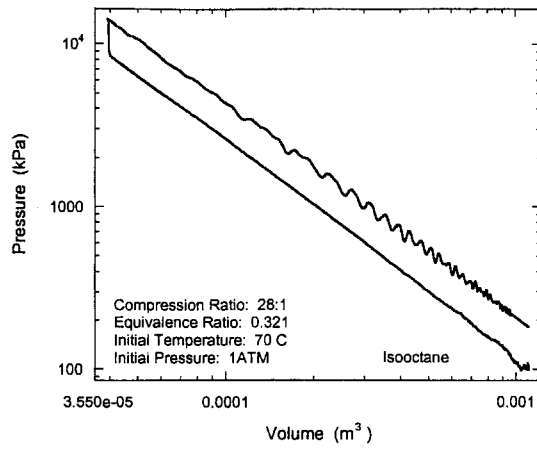


Figure 27 - Isooctane, log pressure vs. log volume.

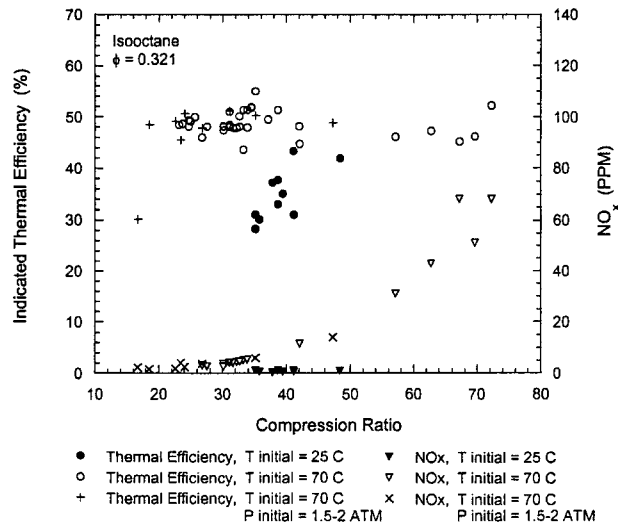


Figure 28 - Isooctane, indicated thermal efficiency and  $\text{NO}_x$  emissions vs. compression ratio.

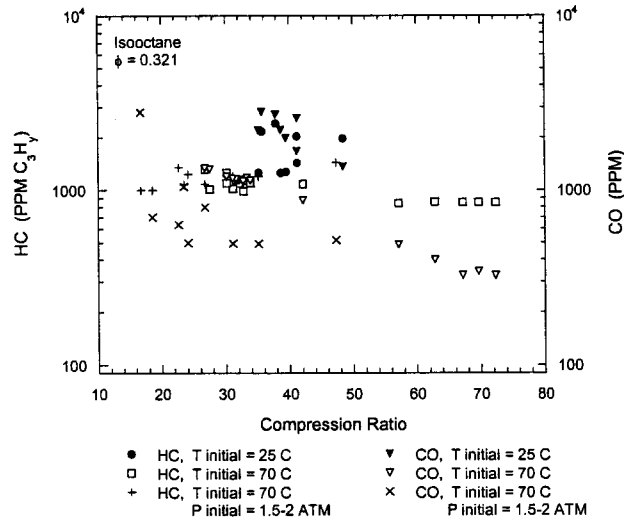


Figure 29 - Isooctane, HC and CO emissions vs. compression ratio.

Comparison of these results to actual engine data, however, must be done with great caution since the intake and exhaust processes are not included, and the fuel/air mixture is completely homogeneous and quiescent before the compression stroke. However, the following trends are noted for the free piston, HCCI combustion process:

High compression ratio can be achieved at the time of combustion. While the initial temperature and fuel type have a strong effect on the compression ratio at which the combustion reactions begin, compression ratios above 30:1 seem achievable for practical operating conditions (e.g., inlet temperature, etc.). The data are unclear regarding efficiency improvements with increased compression ratio, though this could be due to the range of starting temperatures used and the variation with the different fuels investigated.

The high rate of combustion in many cases approaches the constant volume combustion condition. This is especially true for the fuels which have a single stage combustion process (propane, natural gas, hydrogen, methanol, and isooctane).

Over-compression of the cylinder gases after autoignition occurs does not seem to significantly affect the cycle thermal efficiency. While it is possible that greater heat losses are balanced by an increase in the extent to which the fuel/air mixture reacts to completion, this effect cannot be large since the greatest heat release occurs earlier in the compression stroke. This seems to indicate that heat losses do not significantly increase with over-compression. This conclusion is justified by the fact that operation of the experiment without

the piston and cylinder head insulation coatings resulted in an efficiency only 5% less than the insulated runs.

NO<sub>x</sub> emissions do increase with over-compression. This is due mainly to the increased temperatures that result, or the increased time that the cylinder gases spend at higher temperatures.

NO<sub>x</sub> emissions can be sufficiently controlled by decreasing the equivalence ratio, since the problems of spark igniting ultra lean mixtures are not of concern in the HCCI combustion process. HC and CO emissions are present in varying degree, but increasing the initial temperature generally seems to reduce these emissions.

The autoignition characteristics of the fuels tested in these experiments varied widely, and as such the efficiency and emissions results differed significantly. As the data shows some fuels do not react completely, or react in two steps. Generally, higher initial temperatures and higher compression ratios were required to burn more of the fuel to completion. An additional factor that may affect the burning process, especially for the two stage fuels, is the rate of piston oscillation. This variable should be investigated in the future.

The oxidation catalyst performance on these emissions should be investigated in the future. An interesting possibility for emissions control would be to utilize 50% internal EGR (i.e. leave 50% of the combustion products in the cylinder) and add a stoichiometric fresh charge to the remaining cylinder volume. Such an operating strategy with a three-way catalyst could be very attractive. A test series investigating this option was performed with propane where the emissions after 4 cycles were measured. NO<sub>x</sub> was 130 PPM, CO 1720 PPM and HC 360 PPM. The indicated thermal efficiency was 50%.

Current research with HCCI combustion in crankshaft driven engines have shown results similar to ours. Christensen et al<sup>15</sup> evaluated isooctane, ethanol and natural gas in a 1.6 liter displacement single cylinder research engine at a fixed 21:1 compression ratio, at a speed of 1000 RPM. Their efficiency results (not including the inlet/exhaust strokes) using similar equivalence ratios are over 50%.

This research raises the question as to the importance of the free piston geometry to this combustion concept. Certainly the lack of massive kinematic constraints is attractive for such high compression ratios, and the electronic control of compression

ratio broadens the operating range. However, the increased compression ratio possible with the free piston at the time of combustion may not provide much advantage. In the future the performance of the combustion system using a free piston and a crankshaft driven piston under identical operating condition will be compared.

Finally, our work, as well as Christensen's, adds further credibility to the explanation of timing loss as the main cause for real cycle departure from ideal cycle performance as compression ratio is increased.

## Linear Alternator

### Fundamental Questions

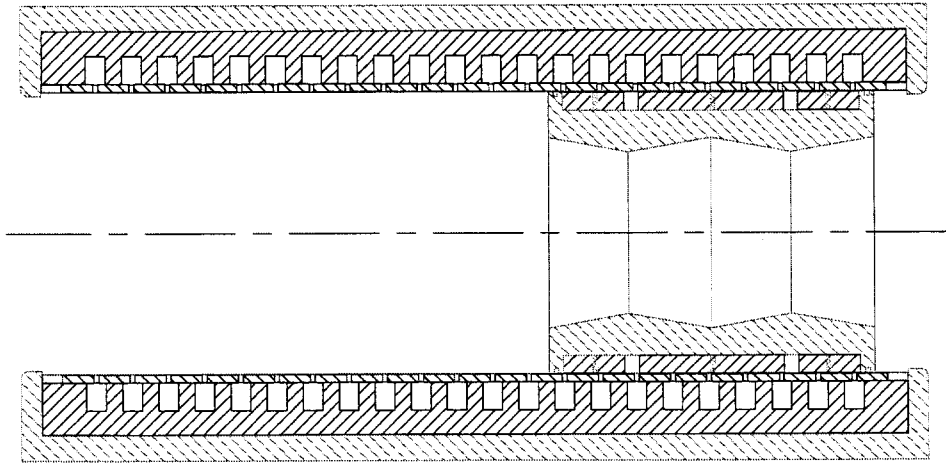


Figure 30 - Cutaway of the linear alternator.

A critical component of the rapid reaction homogeneous charge compression ignition free piston generator concept is the linear alternator. This component is responsible for power generation, starting, and control of the device. Key questions in this study were:

1. Is a linear alternator fundamentally capable of mechanical to electrical conversion efficiencies comparable to rotary devices (95%) ?

2. Can an efficient alternator also be used as a starter motor?
3. Can the power generation rate be controlled to maintain the desired compression ratio ?

## Efficiency

A review of rotary electrical machines indicated that moving permanent magnet devices are the highest efficiency generators. Since the magnetic flux required to generate power does not have to be electrically produced, the main loss terms are the ohmic heating of the output power coils and magnet leakage fields. For example Fisher Electric Technology produces both alternators and motors with efficiencies of 95% at optimal conditions. Review of the Fisher patents (4,900,965, 5,004,944, 5,212,419, 5,311,092, 5,319,844 ) reinforces that a similar flux management system can be built for a linear geometry, probably with greater simplicity. Converting the rotary geometry to a linear configuration should not introduce any additional loss terms, although the equivalent power unit will be somewhat larger due to the low velocity of the moving magnets near the ends of travel. Fisher Electric Technology has provided Sandia with a quote to fabricate a 30kW linear alternator. The dimensions of 7.7 inches in diameter by 8.8 inches long compare quite favorably with rotary devices. At this time we are investigating the design internally to understand the important design constraints.

# Alternator Design

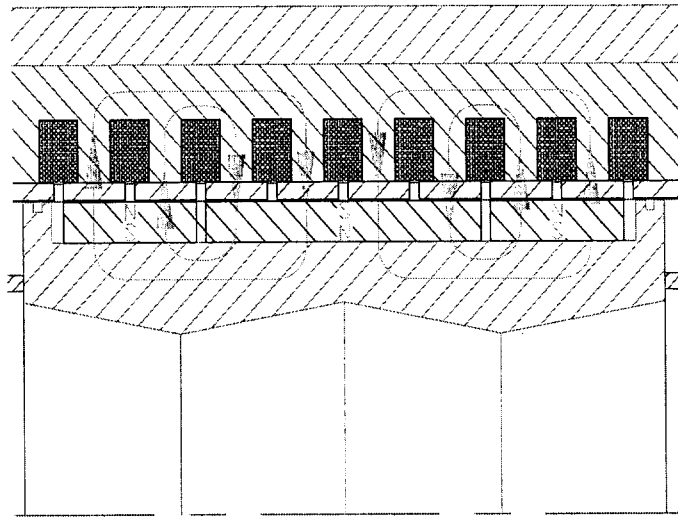


Figure 31 - Flux generation cutaway.

The permanent magnet flux generation design concept is shown in cross section in Figure 31. The three pieces with N and S represent three rare earth permanent ring magnets with radial magnetization. Each ring consists of 8 - 45 degree cylindrical sectors. Each ring will be overwound with soft magnetic steel wire to hold it in place. Note that the direction of magnetization of the center magnet is opposite to the end magnets. We are procuring neodymium iron boron magnets with a minimum energy product of 35 MGO and a maximum working temperature of 150 C. The lines with arrows represent magnetic flux lines generated by these magnets in the moving and fixed steel parts, and passing around the coils. As the magnets are moved axially each of the 22 coils will experience time-varying magnetic fields and thus generate voltages, as explained by Faraday's law of electromagnetic induction. Power is generated when a load is switched onto the coil. Each coil will be isolated from all other coils and all of the voltage rectified to DC. The power will then be stored in batteries. Figure 32 illustrates the generator circuit associated with each alternator coil.

The induced voltage waveform from the coils of a linear alternator is quite different from that of a rotary device. Since a rotary machine can operate at a constant speed, its resulting output is a clean voltage waveform. But because the generation of voltage is based upon the relative motion between the conductor and magnetic flux, or reciprocating motion of the

piston, the changes in speed in a linear device cause distortions in the voltage waveform. To obtain useful power, a full bridge rectifier is used to force the voltage waveform to one polarity, while a capacitor and regulator are used to reduce and eliminate any voltage ripple.

To further our understanding of the important design parameters in building a linear alternator we are analyzing the design with a commercially available computer code called FLUX2D™ by Magsoft Corporation. The code solves Maxwell's equations utilizing the finite element method. It possesses the capability to analyze linear motion and calculates the forces, power output and electrical conversion efficiencies. Los Alamos National Laboratory uses this code extensively and recommended the product to us. We are currently investigating the performance of the design as a function of magnetic circuit parameters.

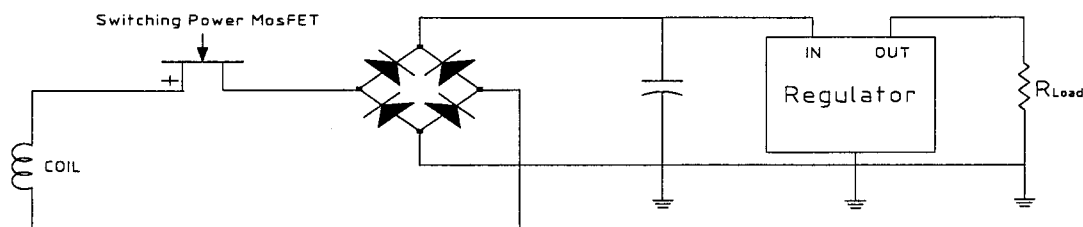


Figure 32. Alternator coil circuit in generator mode.

The alternator is used to control engine operation in the following fashion. Removal of power slows the piston velocity as described by the physical phenomenon of the conservation of energy. By removing more power from the system the piston travels slower towards the end of the cylinder. The control over the piston velocity therefore allows control of the compression ratio. Switching the appropriate number of coils to generate power will be the means of maintaining sufficient CR to sustain the HCCI cycle.

## Starter Motor

As rotary permanent magnet brushless generators can also be operated as motors, the linear design can clearly be utilized to move the piston. Referencing Figure 31, energizing the proper

sequence of coils causes magnetic fields created around the coils to act upon the magnet fields of the rings on the piston. This resultant magnetic force acting on the piston causes the piston to move along the cylinder. The resultant compression of the gas in the cylinder will cause the piston to bounce and proceed in the opposite direction. By controlling the sequence of energizing the coils, the piston can be oscillated back and forth along the cylinder until it reaches a velocity, and thus compression ratio, high enough for autoignition.

## **Control System**

As illustrated from the previous sections describing the linear alternator, an important aspect of the device is control. The system must be able to control the compression ratio of the piston through switching of the coils in power removal, and be able to control the sequence of coil energizing to produce a force upon the piston to move it to start the HCCI cycle.

Design of the control system begins with a model that can simulate the physical phenomenon. This model has been developed with the MATLAB™ application SIMULINK™. The SIMULINK™ model describes and predicts the behavior of the system. The simulation also allows the user to chose the appropriate sensor data to use to control the system.

Once the simulation is complete the control system can then be implemented by a micro-controller or DSP card.

## **Linear Alternator Testing**

In conjunction with the linear alternator design effort we are fabricating an alternator test and permanent magnet characterization capability. A Caterpillar 3304 four cylinder diesel engine has been modified to drive the alternator by attachment of the moving magnets to one of the pistons (see Figure 32). The power input will come from operation of the remaining 3 cylinders. By measuring the appropriate forces, rates and electrical power generation the alternator can be characterized for conversion efficiency. The magnets will separately be subject to shock and thermal loading to determine if such treatment is detrimental to magnet strength or life.

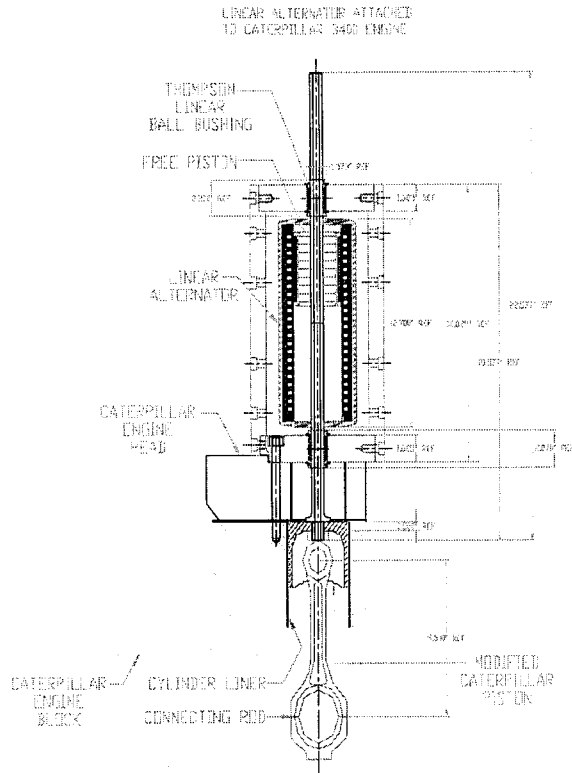


Figure 33. Linear alternator test assembly.

# FREE PISTON ENGINE MODEL

## Model Configuration

In order to investigate the operating characteristics of the free piston engine, a full-cycle, thermodynamic model was developed<sup>23</sup>. This zero-dimensional model consisted of two parts: one to calculate the thermodynamics of the engine cycle, and another to describe the motion of the free piston. A detailed analysis of the changing piston dynamics was necessary since the piston's motion could not be prescribed a priori.

The thermodynamic analysis of the engine cycle includes the compression, combustion, expansion and gas exchange phases, and accounts for heat exchange between the cylinder gases and the cylinder walls. Detailed chemical kinetics are used to describe the HCCI process, while empirical models are employed for the scavenging and heat transfer processes. The free piston analysis couples the calculated cylinder pressure differential with an empirical model for the piston ring-wall friction, and a semi-empirical model for the electromagnetic forces generated by the linear alternator. The details of the alternator, however, are not considered.

Cycle simulations, using hydrogen as the fuel, have indicated the critical factors affecting the engine's performance. The limits of improvement possible relative to conventional IC engine technologies have also been suggested.

## MODEL RESULTS

Typical operating characteristics of the free piston engine as predicted by the engine model are presented first. Figures 34 and 35 depict the piston dynamics where typical position vs. time and velocity vs. position curves are plotted. Illustrated in these figures are the differences between the free piston motion and the motion of a crankshaft-driven piston of the same stroke and maximum piston velocity. For this comparison it is assumed that the ratio of the connecting rod length to the crank radius for the crankshaft driven piston, is 2.5:1.

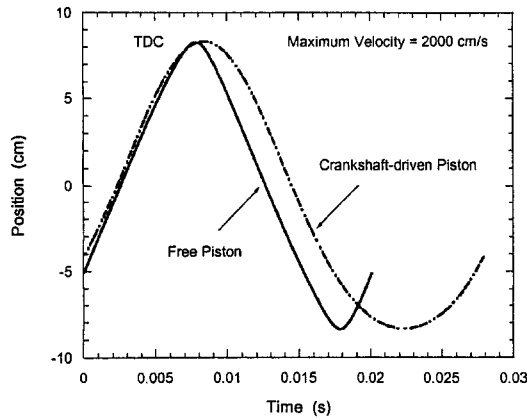


Figure 34. Piston position vs. time for the free piston and a crankshaft-driven piston (stroke - 16.4 cm, maximum velocity - 2000 cm/s).

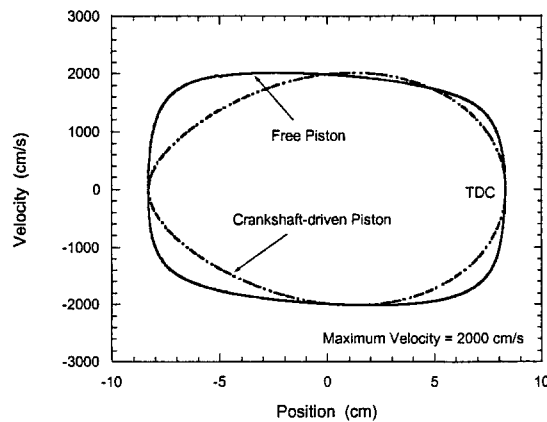


Figure 35. Piston velocity vs. piston position for the free piston and a crankshaft-driven piston (stroke - 16.4 cm, maximum velocity - 2000 cm/s).

It can be seen in Figure 34 that the free piston spends less time at TDC relative to the crankshaft-driven piston. This is illustrated in Figure 35 as well where it is seen that the free piston accelerates and decelerates much more quickly at the ends of each stroke. This inherent characteristic of the free piston can be important in terms of heat transfer losses and  $\text{NO}_x$  formation since shorter residence times at higher temperatures are desirable.

Figure 36 plots a typical pressure vs. time curve for the hydrogen-fueled engine. The pressure plotted here is non-dimensionalized using the scavenged pressure ( $P_{scav}$ ), the pressure at port closure. Figure 37 plots a log pressure vs. log volume curve for the free piston engine cycle. The volume is non-dimensionalized using the engine's displaced volume,  $V_d$ . It can be seen in these figures that the engine model predicts very rapid combustion for the autoignition process, almost constant-volume. The combustion duration, as determined from the rate of pressure increase, is on the order of 10-50  $\mu$ s. This calculation agrees with the results obtained from the RCEM experiments.

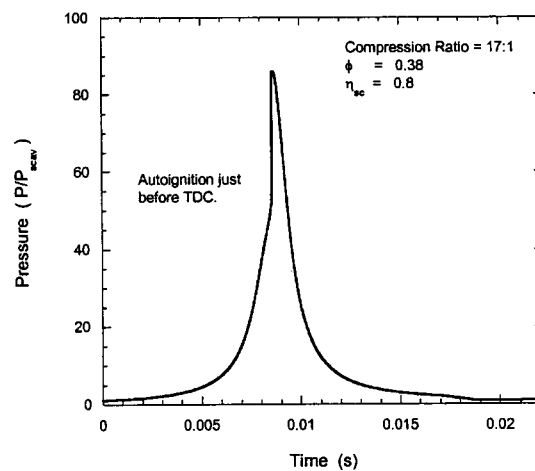


Figure 36. Pressure vs. time.

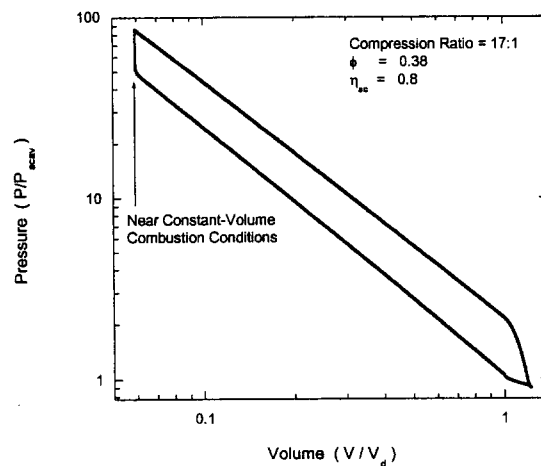


Figure 37. Log pressure vs. log volume.

## Variations in Equivalence Ratio and Scavenging Efficiency

To determine the range of operation and limits of performance for this engine, simulations were conducted at equivalence ratios of 0.15, 0.30, 0.45 and 0.60, and at scavenging efficiencies of 0.5, 0.7 and 0.9. Here the equivalence ratio is defined as ratio of the actual fuel to air ratio to the stoichiometric ratio. The scavenging efficiency ( $\eta_{sc}$ ) is defined as the mass fraction of fresh charge in the cylinder at port closure. The scavenging efficiency was adjusted by fixing the intake and exhaust port conditions.

It should be repeated here that the free piston engine is designed to operate over a range of compression ratios where the optimal steady state operation occurs when the piston compresses the cylinder gases just to the point that they autoignite. Additional compression after combustion is usually not required. The operating compression ratio of the engine is dependent on its operating parameters, as adjusted to provide the amount of compression heating required for autoignition. For these simulations the extent of piston compression was controlled by adjusting the linear alternator's strength so that combustion would occur at or just before TDC. Some variation was allowed in this constraint due to the convergence criteria of the computer code employed. The following discussion is based on simulations where the operating compression ratio was controlled to within +15% greater than the compression ratio required for TDC autoignition.

Figures 38 and 39 illustrate the variations in operating compression ratio with equivalence ratio and scavenging efficiency, respectively. As can be seen, increased equivalence ratios lower the achievable compression ratio, while increased scavenging efficiencies raise the operating compression ratio. These characteristics are due mainly to the effect that  $\Phi$  and  $\eta_{sc}$  have on the temperature of the cylinder gases at the start of compression. This is described as follows.

Increased equivalence ratios lead to higher combustion temperatures which result in more heat per unit mass at the end of the cycle. For a fixed scavenging efficiency, this leads to higher scavenged temperatures. (The effect of equivalence ratio on the compression ratio required for autoignition is secondary to the scavenged temperature effect.)

On the other hand increased scavenging efficiencies result in a greater fraction of fresh charge at the start of compression, and thus a lower thermal mass. A greater percentage of the hot combustion gases is removed from the cylinder with increased scavenging. Although increased scavenging efficiencies lead to higher charge energy densities, due to the fact that there is less dilution by residual gases, the dominant effect is the reduction in scavenged temperature. These points are clearly illustrated in Figure 40 where the engine's operating compression ratio is plotted versus the scavenged temperature.

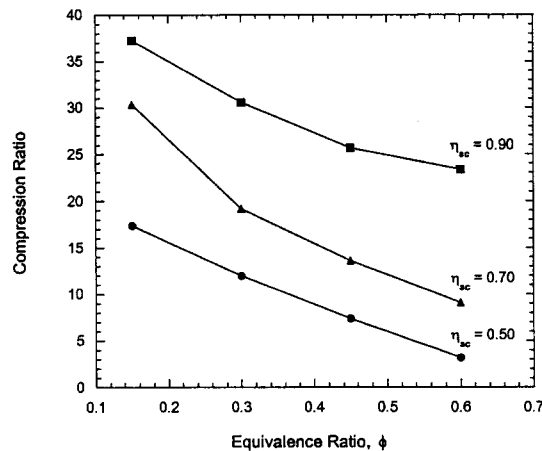


Figure 38. Compression ratio vs. equivalence ratio for various scavenging efficiencies.

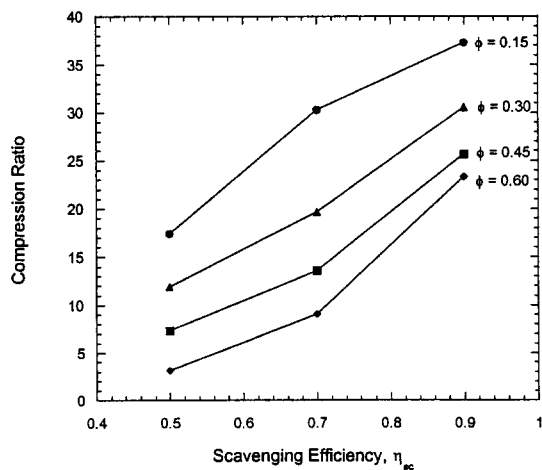


Figure 39. Compression ratio vs. scavenging efficiency for various equivalence ratios.

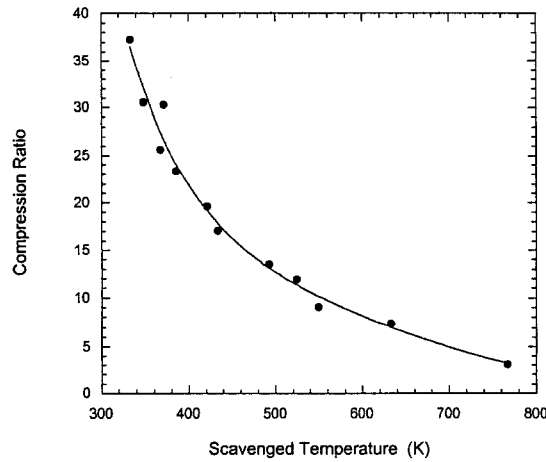


Figure 40. Compression ratio vs. scavenged temperature.

Figure 41 shows the variation in cycle thermal efficiency with operating compression ratio. Here the cycle thermal efficiency is defined as the ratio of the engine's indicated work output, as determined by integrating the pressure-volume curve, to the fuel energy trapped in the cylinder at port closure. This efficiency does not account for the fuel lost through short-circuiting, where unburned fuel escapes through the exhaust port, however, this will be discussed shortly. As expected, the engine's cycle thermal efficiency increases with increased operating compression ratio.

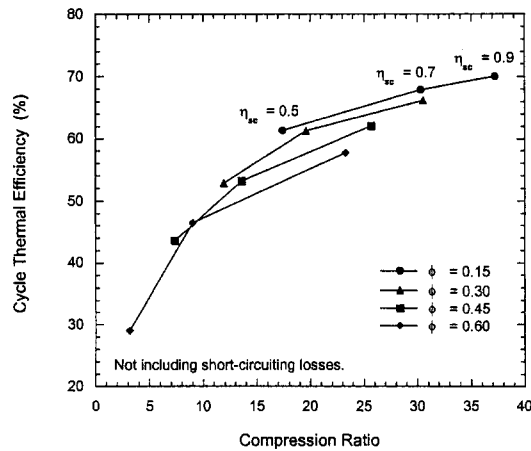


Figure 41. Cycle thermal efficiency vs. compression ratio.

It appears then that both the equivalence ratio and scavenging efficiency significantly affect the achievable indicated thermal efficiencies of this engine through the scavenged temperature. Improvements in the specific heat ratio due to decreased

equivalence ratios and reduced scavenging also contribute to the thermal efficiency increases, although this effect is of secondary importance here.

However Extremely low equivalence ratio operation will prove impractical due to frictional losses in the engine. Additionally, short-circuiting losses will tend to degrade the engine's cycle thermal efficiency for highly scavenged operation, as more fresh gas is required to push the burned charge more completely from the engine. These points will have to be investigated, however the following plot is offered to illustrate the extent to which short-circuiting can negate the improvements in cycle thermal efficiency gained by increased scavenging efficiencies. In Figure 42 the engine's overall efficiency is plotted versus its operating compression ratio. Here the overall efficiency is defined as the ratio of the engine's indicated power output to the fuel energy flow through the engine.

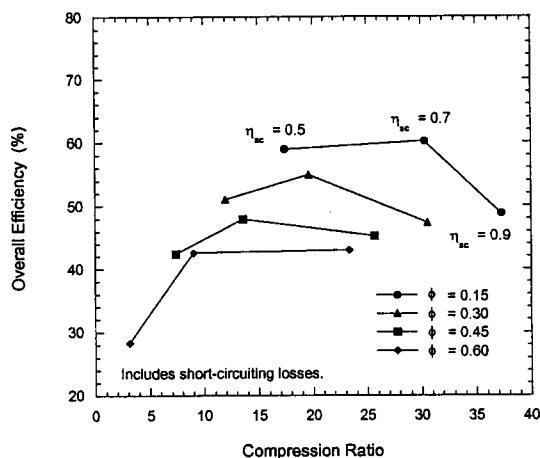


Figure 42. Overall efficiency vs. compression ratio.

In examining this plot it should be noted that the empirical model used to describe the scavenging process tends to predict significant increases in fuel short-circuiting for highly scavenged systems. This problem can be addressed, however, in the engine design through fuel injection techniques or stratified scavenging. The potential for these solutions was not investigated in these simulations.

The pollutant emissions potential of the free piston engine are presented next. Here only the  $\text{NO}_x$  emissions are given since hydrogen was used as the fuel. As stated earlier, emissions of unburned hydrocarbons and carbon monoxide from operation with other fuels are expected to be controlled using oxidation catalyst technologies.

The  $\text{NO}_x$  performance is characterized in this study based on the dilution ratio, as opposed to the equivalence ratio. This is due to the fact that the scavenging efficiencies dictate the amount of the fresh charge fuel energy that is trapped in the cylinder at port closure, and this may be quite different than the intake equivalence ratio. The dilution ratio is defined here as the ratio of the actual fuel to air plus residual gases ratio to the stoichiometric fuel to air ratio.

Figure 43 illustrates how the  $\text{NO}_x$  concentrations increase with increasing dilution ratio. In these results the  $\text{NO}_x$  levels include  $\text{NO}$ ,  $\text{NO}_2$ , and  $\text{N}_2\text{O}$  emissions, though  $\text{NO}$  was the predominant species. The increases in  $\text{NO}_x$  with dilution ratio are due mainly to the increased combustion temperatures that result from higher charge energy densities. The scatter in the simulated points in this figure seems to be primarily a function of over-compression of the cylinder charge after autoignition, as discussed previously.

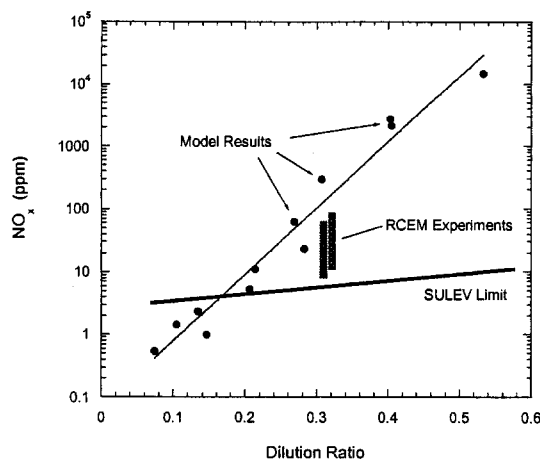


Figure 43.  $\text{NO}_x$  vs. dilution ratio.

Also shown in Figure 43 are selected results from the RCEM experiments using hydrogen. The scatter in the experimental data is due to both over- and under-compression of the cylinder charge. Reasonable agreement is reached between the simulated points and the data where the discrepancies are most likely due to the model's uniform charge assumption, and the inadequacy of the heat transfer model used.

Finally, shown in Figure 43 is CARB proposed Super Ultra Low Emissions Vehicle (SULEV)  $\text{NO}_x$  standard<sup>24</sup>. (This  $\text{NO}_x$  limit assumes a vehicle efficiency of 60 miles per gallon.) The SULEV standard is the goal that should be met by any advanced IC engine designed

for reduced emissions. From Figure 43 it is clear that there is a limit of operation for compliance.

The following studies were conducted at a dilution ratio of 0.2 since this appeared to be within the range of compliance of the SULEV standard, extrapolating from the experimental data for the kinetic modeling. Actual operation could probably be greater than 0.2, since the model tends to over predict the  $\text{NO}_x$  emissions.

## Control of the Scavenged Temperature

Figure 40 illustrated the detrimental effect high scavenged temperatures have on the operating compression ratio of this engine. The corresponding decrease in cycle thermal efficiency was presented in Figure 41. In order to reduce the scavenged temperatures high scavenging efficiencies could be used. However increased short-circuiting, as predicted by the empirical scavenging model, would probably negate any improvements. This is illustrated in Figure 44 where the cycle thermal efficiency and overall efficiency are plotted versus the scavenging efficiency. The short-circuiting ratio, defined here as the mass fraction of fresh charge that leaves the cylinder before port closure, is included for reference. This ratio provides an indication of the amount of fresh gas that must be sacrificed to remove increasing amounts of burned charge from the cylinder.

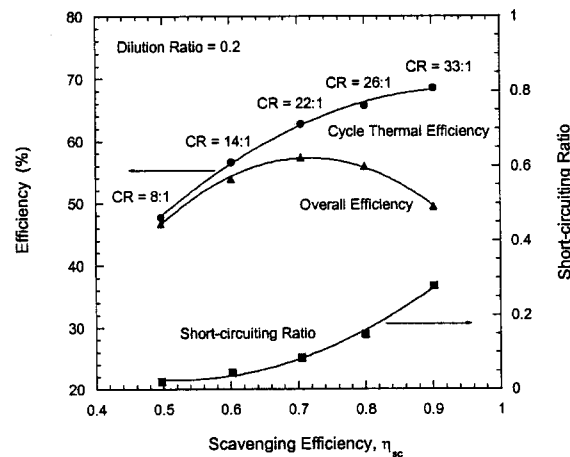


Figure 44. Cycle thermal efficiency, overall efficiency, and short-circuiting ratio vs. scavenging efficiency.

The use of low scavenging efficiencies, along with sufficient control of the scavenged temperatures by reduced intake temperatures, in order to improve the overall efficiency of the

engine was investigated. Several scavenging efficiencies were studied, where the cylinder charge was diluted by varying fractions of residual gases and intake air. Figure 45 illustrates the variation in cycle thermal efficiency and overall efficiency with scavenging efficiency. Here the scavenged temperature was maintained at 340 K. The operating compression ratio in these runs was 35:1.

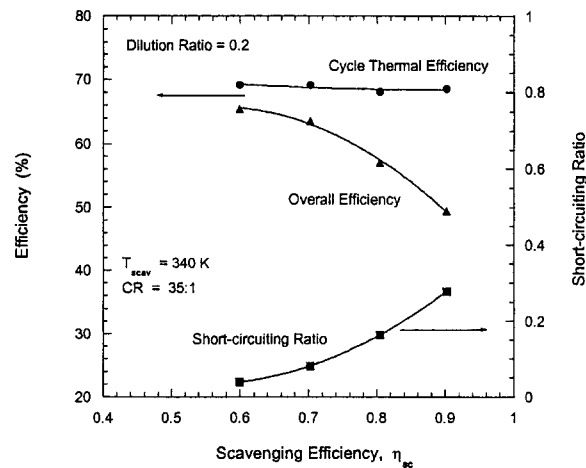


Figure 45. Cycle thermal efficiency, overall efficiency, and short-circuiting ratio vs. scavenging efficiency.

Figure 45 shows that the cycle thermal efficiency remains relatively constant for the various scavenging efficiencies investigated. It appears that operation on high fractions of residual charge can yield equivalent thermal efficiencies as low equivalence ratio operation (for the same overall dilution ratio), as long as high compression ratios can be reached. As a result, thermal control of the cylinder charge in conjunction with reduced scavenging could be used to increase the cycle thermal efficiency, and thus the corresponding overall efficiency.

## Compression Ratio Control

The free piston design of this engine offers a reduction in the number of moving parts and reduced mechanical friction. However, this is at the cost of sophisticated electronic control. The absence of mechanical linkages necessitates the ability of the linear alternator to moderate the free piston dynamics through each and every stroke such that the required compression ratio is achieved.

As can be inferred from the scatter in Figure 43, variations in charge over-compression can affect the  $\text{NO}_x$  emissions of this engine. To determine the extent to which this is a critical parameter, the engine code was used to investigate the over- and under-compression of the cylinder charge and the subsequent effects on the engine's cycle thermal efficiency and  $\text{NO}_x$  emissions. The range of piston motion was controlled by adjusting the alternator strength. A constant intake temperature of 300 K was used, and the simulated cycle was operated at a scavenging efficiency of 0.8. Dilution ratios of 0.2 and 0.3 were investigated.

Figures 46 and 47 illustrate the effects of variations in the piston motion. The cycle thermal efficiency and  $\text{NO}_x$  emissions are plotted versus operating compression ratio, where this represents the compression ratio achieved by the engine, though this can be greater than that required for TDC autoignition. Figure 46 shows little variation in the cycle thermal efficiency over the range investigated, as long as the piston motion leads to proper autoignition and complete combustion. This seems to indicate that heat loss near TDC is not greatly affected by small changes in the piston's dynamics, even though significantly increased pressures result. This finding is supported by the experimental results<sup>25</sup>. On the other hand  $\text{NO}_x$  emissions were found to be very sensitive to the range of over or under-compression, increasing in orders of magnitude for variations in the piston motion of only 1-2% of the entire piston stroke. This appears to be attributable to the higher temperatures seen with increased compression.

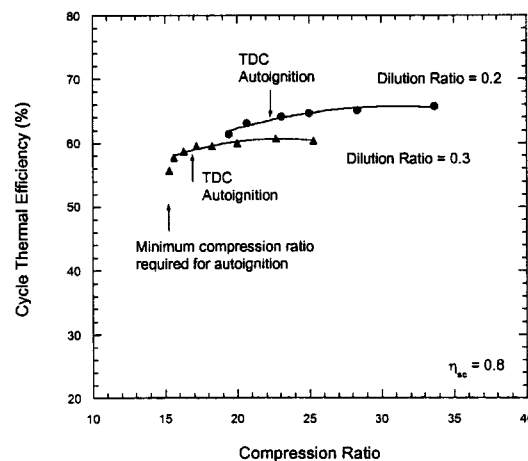


Figure 46. Cycle thermal efficiency vs. compression ratio.

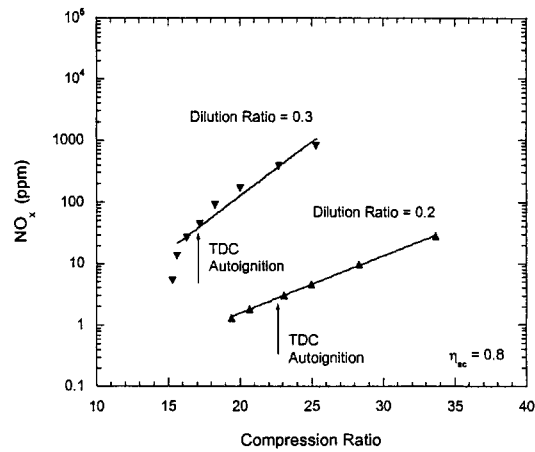


Figure 47. NO<sub>x</sub> vs. compression ratio.

## Model Discussion

The free piston engine model allows the engine cycle to be simulated over a range of operating conditions, thus enabling a thorough investigation of the free piston engine's steady-state characteristics. However, care must be taken when interpreting the model's results. Limitations within the model include the following assumptions: zero-dimensional characterization of the in-cylinder processes, and the applicability of the empirical heat transfer, scavenging, and friction models employed.

The engine simulation results are next compared to the performance of conventional spark-ignition and compression-ignition IC engines. Achieving almost constant-volume combustion, capable of operating on very lean mixtures, and utilizing very high compression ratios, the proposed free piston engine operating on hydrogen, seems to meet the requirements for optimized Otto cycle operation.

The simulation results, based on the model parameters, indicate that this engine is capable of achieving individual ideal cycle thermal efficiencies near 65% (55% confirmed through the RCEM experiments<sup>26</sup>), while complying with proposed SULEV NO<sub>x</sub> emissions standards. This is a gain in cycle thermal efficiency of 35% over conventional Diesel engines and nearly 70% over conventional spark-ignition engines. Further, the possibility of stringent NO<sub>x</sub> emissions compliance without the need for exhaust gas after-treatment seems to be an inherent capability of the free piston engine operating on very lean mixtures<sup>27</sup>. Eliminating the need

for massive or mechanically complex designs, the free piston engine poses a significant advancement in IC engine technology.

## Scavenging System

### Scavenging Background

Two-stroke cycle scavenging is required for the free piston engine's operation. Successful preparation of the cylinder charge for the HCCI combustion process, and control of short-circuiting losses will be critical to ensuring the efficiency and emissions potential of the engine.

Conventional two-stroke engines are notorious for high hydrocarbon emissions, and excessive fuel consumption. This is mainly due to the large quantities of unburned fuel lost through the exhaust port during the gas exchange process. Further, variations in the incoming charge over the range of engine operating speeds can affect the quality (homogeneity) of the cylinder charge at top dead center. Large fractions of residual gases can also affect the combustion process.

Advances in two-stroke technology have led to improvements in fuel economy and engine emissions. Alternative fuel introduction schemes such as direct cylinder injection, and stratified scavenging have enabled short-circuiting losses to be reduced, while optimization of the cylinder/port geometries, and port timings have improved the charge preparation in many two-stroke cycle engines.

Within the free piston engine it is expected that the scavenging system will be similar to that used in conventional two-stroke cycle engines. However, differences should arise due to the limited range of piston speeds over which the engine will operate, and the high residual gas fractions that may be tolerated by both the HCCI combustion system and the engine's electrical power requirements.

The objective of the proposed work is to develop a scavenging system suitable to the free piston engine, capable of ensuring that the HCCI combustion system's efficiency and emissions potential are not degraded through the gas transfer process. Factors influencing the performance of this system under typical engine operation will be investigated.

## Design Approach

Conventional scavenging configurations are of the loop, cross-flow, or uniflow type. Crankcase compression or external blowers generally drive the flow. These scavenging systems, and their incorporation into crankshaft-driven engines have evolved significantly over time. Substantial experimental data has been collected, and numerous empirical methods developed. Modern systems are designed based on the requirements of wide operating ranges, high power output, and more recently, controlled emissions.

Various experimental tools have been used in the design of the two-stroke cycle scavenging system. These include the Jante test, in-cylinder and exhaust gas composition analysis, single-shot and continuous visualization, as well as non-intrusive, in-cylinder fluid dynamic measurements. More recently, computational analyses have been incorporated into the design process. Zero-dimensional and multi-dimensional models have been used to complete parametric studies, and to gain a better understanding of the in-cylinder flow patterns.

In the proposed analysis, computational methods will be employed as the principal design tool. A multi-dimensional code (KIVA) will be used to create an initial design for the scavenging system. The influence of parameters such as the port/valve geometry/timing, intake/exhaust conditions, cylinder geometry, fuel introduction, and free piston dynamics will be investigated. A range of operating conditions (fuel type, equivalence ratio, etc.) is to be studied. Both the short-circuiting problem and the issue of charge preparation will be analyzed.

The computational effort will be accompanied by an experimental program that will seek to validate the computer code's results. A single-shot, free piston-cylinder device will be constructed to simulate the engine's gas exchange process. An abbreviated stroke (port open to port close), with the possibility of the complete compression stroke, will be used.

Both uniflow and loop scavenging designs are to be investigated, with an electromagnetic valve used for the uniflow design. Various port/valve geometries will be studied. Different fuel introduction schemes will also be investigated. Measurements of the in-cylinder, and intake/exhaust pressures, as well as the overall scavenging and trapping efficiencies will be used to compare the experimental findings with the computational results.

Video recording of the process should aid in qualitatively assessing the validity of the predicted results. Measurement of the exhaust gas composition through the gas transfer process may also be used to check the calculated results.

It is expected that heated air (with known NOx concentrations), at reasonable blowdown pressures, will be used to simulate the combustion products. Cool air (containing fixed concentrations of a hydrocarbon compound) will be used to simulate the fresh incoming charge. Seeding of the intake charge may be required for proper video imaging.

The piston used in the experiment will be driven by the free piston of a rapid compression expansion machine. The free piston dynamics may be an important consideration in this design problem.

## Conclusion

This report presents the results of an investigation conducted to determine if a new combustion driven approach to electricity generation can result in both higher conversion efficiency and lower emissions than current technology. Investigation of the combustion system, electrical power generation and control system algorithms have been presented as well as the results from extensive system modeling.

These investigations positively support the hypothesis that improved performance is possible. Based on this supporting evidence a fuel to electricity conversion efficiency of 50% is projected in a small (30 KW ) device. An added benefit is the low emissions capability through existing oxidation catalyst technology.

A patent of the free piston / homogeneous charge compression ignition device was applied for in June of 1998.

# REFERENCES

1. Edson, M. H. and Taylor, C. F., "The Limits of Engine Performance - Comparison of Actual and Theoretical Cycles," Digital Calculations of Engine Cycles, SAE Prog. in Technology, vol. 7, pp.65-81, 1964.
2. Van Blarigan, P., "Development of a Hydrogen Fueled Internal Combustion Engine Designed for Single Speed/Power Operation," SAE Paper 961690, 1996.
3. Edson, M. H., "The Influence of Compression Ratio and Dissociation on Ideal Otto Cycle Engine Thermal Efficiency," Digital Calculations of Engine Cycles, SAE Prog. in Technology, vol. 7, pp. 49-64, 1964.
4. Caris, D. F. and Nelson, E. E., "A New Look at High Compression Engines," SAE Transactions, vol. 67, pp. 112-124, 1959.
5. Overington, M. T. and Thring, R. H., "Gasoline Engine Combustion - Turbulence and the Combustion Chamber," SAE Paper 810017, 1981.
6. Muranaka, Y. T. and Ishida, T., "Factors Limiting the Improvement in Thermal Efficiency of S.I. Engine at Higher Compression Ratio," SAE Transactions, vol. 96, section 4, pp. 526-536, 1987.
7. Das, L. M., "Hydrogen Engines: A View of the Past and a Look Into the Future," International Journal of Hydrogen Energy, vol. 15, no. 6, pp. 425 - 443, 1990.
8. Van Blarigan, P. and Green, R., "NO<sub>x</sub> Emission Data Verified in a Hydrogen Fueled Engine," Combustion Research Facility News, vol. 17, no. 4, January/February 1995.
9. Onishi, S., Jo, S. H., Shoda, K., Jo, P. D. and Kato, Satoshi, "Active Thermo-Atmospheric Combustion (ATAC) - A New Combustion Process for Internal Combustion Engines," SAE Paper 790501, 1979.
10. Karim, G. A. and Watson, H. C., "Experimental and Computational Considerations of the Compression Ignition of Homogeneous Fuel-Oxidant Mixtures," SAE Paper 710133, 1971.

## REFERENCES (continued)

11. Alperstein, M., Swim, W. B. and Schweitzer, P. H., "Fumigation Kills Smoke - Improves Diesel Performance," SAE Transactions, vol. 66, pp. 574-588, 1958.
12. Thring, R. H., "Homogeneous-Charge Compression-Ignition Engines," SAE Paper 892068, 1989.
13. Najt, P. M. and Foster, D. E., "Compression-Ignited Homogeneous Charge Combustion," SAE Paper 830264, 1983.
14. Christensen, M., Johansson, B., Amneus, P. and Mauss, F., "Supercharged Homogeneous Charge Compression Ignition," SAE Paper 980787, 1998.
15. Christensen, M., Johansson, B. and Einewall, P., "Homogeneous Charge Compression Ignition (HCCI) Using Isooctane, Ethanol and Natural Gas - A Comparison with Spark Ignition Operation," SAE Paper 972874, 1997.
16. Underwood, A. F., "The GMR 4-4 'Hyprex' Engine - A Concept of the Free-Piston Engine for Automotive Use," SAE Paper 570032, 1957.
17. Klotsch, P., "Ford Free-Piston Engine Development," SAE Paper 590045, 1959.
18. Baruah, P. C., "A Free-Piston Engine Hydraulic Pump for an Automotive Propulsion System," SAE Paper 880658, 1988.
19. Achten, P. A. J., "A Review of Free Piston Engine Concepts," SAE 941776, 1994.
20. Lee, W. and Schaefer, H. J., "Analysis of Local Pressures, Surface Temperatures and Engine Damages under Knock Conditions," SAE Transactions, vol. 92, section 2, pp. 511-523, 1983.
21. Maly, R. R., Klein, R., Peters, N. and Konig, G., "Theoretical and Experimental Investigation of Knock Induced Surface Destruction," SAE Transactions, vol. 99, section 3, pp. 99-137, 1990.
22. Park, P. and Keck, J. C., "Rapid Compression Machine Measurements of Ignition Delays for Primary Reference Fuels," SAE Paper 900027, 1990.

## REFERENCES (continued)

23. Goldsborough, S. S. and Van Blarigan, P., "A Numerical Study of a Free Piston IC Engine Operating on Homogeneous Charge Compression Ignition Combustion," (in press), 1999.
24. Van Blarigan, P., "Development of a Hydrogen Fueled Internal Combustion Engine Designed for Single Speed/Power Operation," SAE Paper 961690, 1996.
25. Van Blarigan, P., Paradiso, N. and Goldsborough, S., "Homogeneous Charge Compression Ignition with a Free Piston: A New Approach to Ideal Otto Cycle Performance," SAE Paper 982484, 1998.
26. Van Blarigan, P., "Advanced Hydrogen Fueled Internal Combustion Engines," *Energy & Fuels*, 12, 72-77, 1998.
27. Goldsborough, S. S., "A Numerical Investigation of a Two-Stroke Cycle, Hydrogen-Fueled, Free Piston Internal Combustion Engine," M.S. Thesis, Colorado State University, Summer 1998.

# APPENDIX

## Rapid Compression Expansion Machine

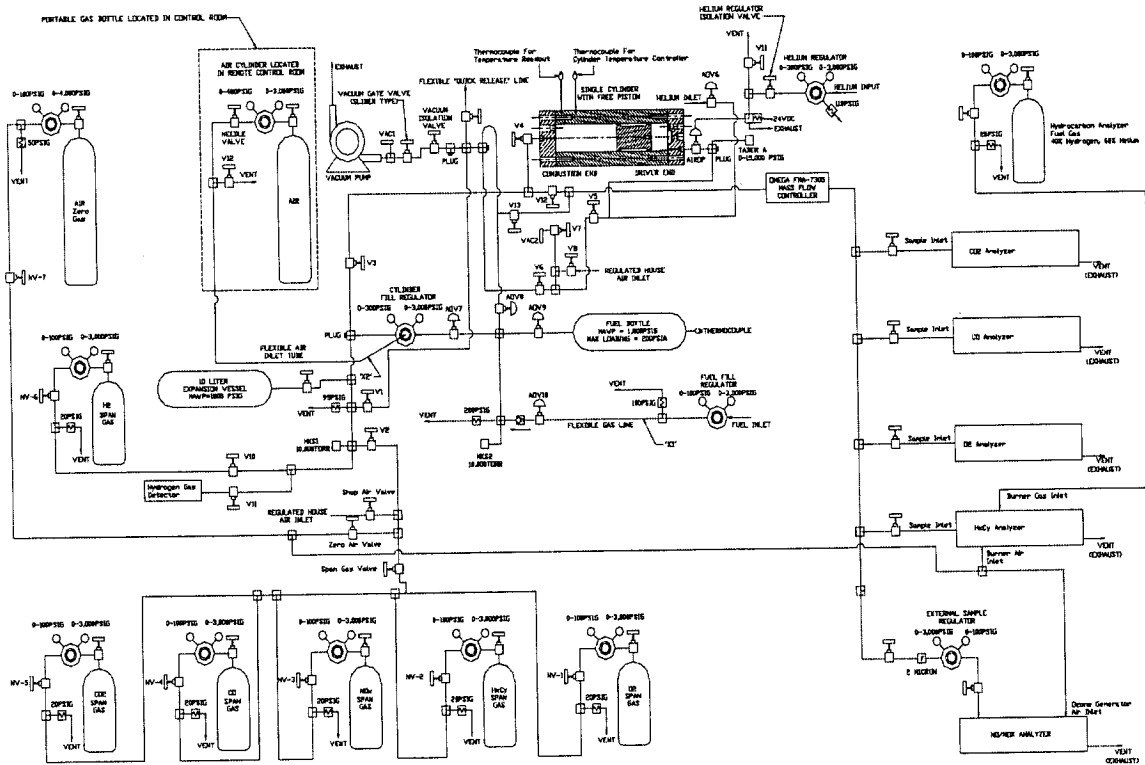


Figure A.1 - Schematic of free piston combustion experiment.

RAPID COMPRESSION EXPANSION MACHINE - A schematic of the RCEM and the experimental setup is illustrated in Figure A.1. The RCEM uses high pressure helium gas to drive a double ended, free piston from one end of a double ended cylinder to the other. This driving motion compresses the initially quiescent fuel/air charge to the point of autoignition. As the combusted gases expand the piston is driven back through the cylinder recompressing the helium driver gas. The piston bounces a few times before coming to rest. The oscillating piston motion from a typical run is illustrated in Figure A.2. Here it can be seen that the piston does not fully return to its initial position due to the compression of the trapped helium gas.

The relevant specifications of the RCEM can be found in Table A.1. A detailed description of the machine's construction and operation follow.

Double-Ended Cylinder - The cylinder section was constructed of 6061-T6 aluminum with the dimensions of 35.56 cm length, 7.62 cm inside diameter, and 15.24 cm outside diameter. The cylinder bore was hard anodized and honed to a finish of 16-32 microinches. The body was wrapped with Briskheat electrical heating tape and covered with FiberFrax insulation to perform heated experiments.

Cylinder Heads - The front and back cylinder heads were constructed of 304 stainless steel. The front head (combustion chamber) contained access ports for two pressure transducers, two surface thermocouples, an air-operated pressure trap, and fuel loading. All pressure transducer holes were centered on a radius of 25 mm. The port for fuel loading was located in the center of the head. The back cylinder head contained access ports for one pressure transducer and the source driver gas. Both cylinder heads were wrapped with Briskheat electrical heating tape, over wrapped with ThermoTec insulation, and then covered with FiberFrax insulation.

Table A.1 - Rapid Compression - Expansion Machine Specifications.

Bore (mm)	76.2
Stroke (mm)	254 max, 236 typical
Displacement (L)	1.076 typical
Cylinder	6061 aluminum, hard anodized
Cylinder Head	304 stainless steel
Piston	303 stainless steel
Maximum Piston Speed (cm/s)	1100 typical
Natural Oscillation Frequency (Hz)	40 typical

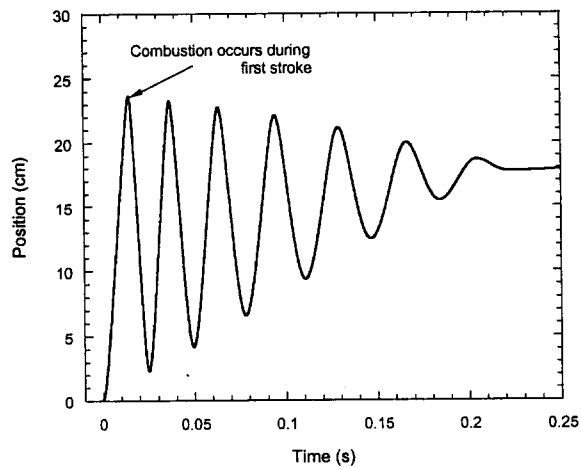


Figure A.2 - Piston position vs. time.

Piston and Seals - The double ended piston was machined from 303 stainless steel to the dimensions of 11.05 cm length and 7.85 cm diameter. The mass of the piston, including the piston seals, was 2.89 kg.

In order to accurately quantify the thermal efficiency of the cycle it was important that the cylinder gases not be lost to leakage from the combustion chamber. In an effort to seal off the front chamber, three different seal configurations were used. These are described in detail below. The final combination represented the best option for the combustion experiment's operation, and produced the most consistent data.

In the first configuration each end of the piston was fitted with one ring seal. A Furon lip seal (part # 250-334-3307) was used in conjunction with a stainless steel expander spring. Additionally, a Teflon sleeve was attached to piston's midsection to improve the piston's movement inside the cylinder. Parker Teflon-impregnated o-rings (part #2-334-V848) were used in place of the Furon seals in some tests.

In the second configuration the piston was fitted with two seals located on the combustion chamber end, and one seal on the driver end. In this design a C. Lee Cook compression ring (part # 559648WGX) was used on the outer combustion chamber end, and behind that, a Furon lip seal (part # 250-334-3307). Here an o-ring was used in the place of the expander spring. On the driver end, a Furon lip seal was used with the stainless steel expander ring. In addition to these outer seals, two C. Lee Cook bronze-impregnated Teflon rider rings (part # 559647MFL) were fitted to

the piston's midsection. Parker Teflon-impregnated o-rings were also used in place of the Furon ring on the combustion chamber end in later tests.

The third seal configuration used two seals on the combustion chamber end and one on the driver end. The outer combustion chamber seal used a Parker orange Teflon ring (part # S-5000-48), and behind that a Furon lip seal (part # 250-334-3307) with an o-ring expander second ring. On the driver end a Furon lip seal was used in conjunction with a stainless steel expander spring. In this configuration, two C. Lee Cook bronze-impregnated Teflon rider rings were used. In later tests a Parker Teflon impregnated o-ring was used in place of the Furon seal on the combustion end.

Due to the changes in the piston/seal mass resulting from the different seal configurations, the piston's center section had to be machined so that the total piston/seal mass of 2.89 kg could be maintained.

Seal Lubrication - In early tests Parker silicone based Super-O-Lube was used to lubricate the o-rings. This lubricant however, was found to partially oxidize during the experimental runs. This was especially noticeable after the hydrogen and isooctane tests. Deposits were found on both the piston and cylinder head, and within the tubing leading to the emissions analyzers. Inaccurate readings of the exhaust emissions and fouled efficiency calculations resulted. The extent to which the emissions data were skewed can be seen in Figure 13, where the HC and CO emissions should have been null.

The use of seal lubrication was discontinued after this finding and the experimental apparatus fully cleaned.

Piston and Cylinder Head Coating - The piston crown and combustion chamber head were coated with Dow Corning Silastic J silicone in order to reduce the heat transfer between the cylinder gases and the combustion chamber surfaces. The details of the application procedure are described below.

The piston and cylinder head were first glass bead blasted to roughen the surface, and then wiped with acetone to remove any contamination. The cylinder head was masked off with a 15.24 cm diameter round plastic adhesive sheet that had a 7.62 cm hole in the center. This mask was used to limit the area covered with Silastic J and to set the depth of the coating. Both parts were primed with Dow Corning P5200 adhesion promoter.

After the primer dried, the silicone was applied to both parts with a spatula. The silicone was also applied to an aluminum blank that had been treated with mold release. The blank had three small pins, each protruding 0.5mm from its surface which were used to maintain a gap between the piston and the blank.

The piston and cylinder head, and blank were then placed in a vacuum chamber to degas the Silastic J. The parts were removed from the vacuum chamber and the piston placed on the aluminum blank. The weight of the piston forced the excess from between the piston and the blank leaving the piston resting on the blank's pins. The coating on the cylinder head was leveled with the mask by drawing a straight edge across the surface.

Both parts were allowed to cure overnight with a final cure the next day in an oven at 60 C for four hours. The coating thickness was verified by slicing the coating from each part with a razor and measuring its thickness with a caliper.

Fuel Mixing - Both liquid and gaseous fuels were tested. For gaseous fuels a premixed charge storage bottle (10 liters) was evacuated to a pressure of 1 Torr or less, and then filled with the fuel to a desired pressure (calculated based on the fuel/air equivalence ratio). When this pressure was reached the bottle was valved off and the contents allowed to achieve a stable temperature. Changes in the fuel's pressure were recorded, and then dry air was slowly added until the total fuel and air pressure reached the required value.

For liquid fuels two methods were used to mix the fuel and air. The first method used a direct cylinder injection technique while the other relied on the use of a premixed storage bottle. A brief description of each follows.

In the first method the combustion chamber was initially filled with dry air to atmospheric pressure and sealed off. The fuel loading port was opened and a small amount of fuel injected directly into the cylinder using a stainless steel syringe. The port was quickly closed and the mass of injected fuel measured on a Mettler AE-163 scale. The fuel was then allowed to completely evaporate. This process lead to variations in the fuel/air equivalence ratio between test runs so a new method of fuel loading was developed.

In the second method the premixed storage bottle was initially evacuated to a pressure of 1 Torr or less. A small container containing liquid fuel was then connected to the storage bottle housing and the fuel allowed to evaporate into the bottle and

pipng. Once the bottle pressure and temperature stabilized the bottle was valved off and the liquid fuel container removed. Dry air was added to the storage bottle until the desired equivalence ratio was reached. Care was taken to ensure that the fuel remained vaporized at room temperature.

Mass spectrometer analysis has verified the precision of each mixing method.

The RCEM was located in a high pressure test cell. The transfer of the combustible gas mixes from the 10 liter fuel/air tank to the experiment cylinder was done remotely, as was the addition of air to the fuel/air storage tank and the firing of the device.

Cylinder Charging - To fuel the experiment the piston was moved to its initial position at the back of the cylinder by use of vacuum and atmospheric pressures. The entire assembly was then evacuated to a pressure of 1 Torr or less, and the premixed fuel/air charge loaded through the fueling port to a cylinder pressure of about 760 Torr.

Piston Driving - The helium driver gas was remotely pumped up to the required driving pressure using a Newport Scientific Aminco pump. The driver gas pressure was typically 362,000-490,000 Torr, depending on the desired compression ratio (higher compression ratios required higher driver pressures). To dump the high pressure helium gas into the driver end of the cylinder, a specially modified Nupro bellows valve actuated with an Autoclave Engineers air operator (also driven by helium) was used. With this configuration the driver supply was quickly released into the back end of the cylinder. Data acquisition was triggered by the rising pressure in the driver end.

Pressure Measurement - The static magnitude of all low pressure gases was measured using two 10,000 Torr absolute pressure range MKS Barratrons, Type 390 HA heads with Type 270B display units achieving an accuracy of 0.05% of reading. High pressure gases (i.e., helium) were measured using Teledyne-Taber strain gauge transducers with an accuracy of 0.25% of full scale.

Dynamic pressures were measured using piezoelectric effect transducers. Pressure on the driver end was quantified with a Kistler Type 607 transducer coupled to a Kistler Type 5004 charge amplifier. The combustion end utilized two transducers. Kistler Type 7061A, 7063A, 7061B, 607L, and AVL Type QC42D-X were employed with Kistler Type 5010 and 5026 charge amplifiers. To improve the accuracy of the combustion pressure measurements the transducers were coated with Dow Corning Silastic J silicone

compound. The application procedure was essentially the same as that used for the piston/cylinder head coating, and is described below.

Pressure data were recorded on three Nicolet 4094 digital oscilloscopes through 12 bit Type 4570 plug-ins, at a rate of 500,000 samples per second.

In order to ensure the accuracy of the combustion chamber pressure record, an additional Teledyne-Taber Type 2210 transducer was added to the cylinder head. This transducer was isolated from the combustion event through the use of an air operated valve. The valve, initially closed, was opened during the first expansion stroke so that the final expansion pressure could be recorded. A Daytronic Type 3270 strain gage conditioner/indicator was used in conjunction with this transducer.

A comparison of the Teledyne-Taber transducer record to the Kistler and AVL records indicated that the AVL unit matched the Teledyne-Taber record better.

Pressure Transducer Coating - The procedure for applying the Silastic J thermal coating to the pressure transducers is described here. The application procedure for the Kistler and AVL pressure transducers was very similar to the piston/head coating procedure. The transducers were first glass bead blasted to roughen the surface, and then wiped with acetone to remove any contamination. The transducers were coated with Dow Corning P5200 adhesion promoter; this promoter was found to work equally well for the plain style stainless steel face transducers and the TiN coated transducers.

After the primer dried the transducers were threaded into a setup fixture and locked with their faces 0.5mm below the surface of the fixture. Silastic J was then applied to the transducers with a spatula. The transducers were placed in a vacuum chamber to degas the Silastic J. The transducers and fixture were then removed from the chamber and the Silastic J leveled by pulling a razor across the surface of the setup fixture. The transducers were then allowed to cure overnight with a final cure the next day in an oven at 60 C for four hours. After the transducers cooled they were removed by slicing the Silastic J around the transducer face and unthreading them from the fixture. The coating thickness was verified by coating one transducer without first priming it. This allowed the cured Silastic J to be peeled from the transducer and its thickness measured with a caliper.

Displacement Measurement - The piston displacement was measured using a Data Instruments FASTAR Model FS5000HP inductive transducer. Data were recorded on a fourth Nicolet 4094 digital oscilloscope at a rate of 200,000 samples per second.

Vibration Measurement - The vibration of the rapid compression-expansion machine was measured using two Endevco Model 2250A M1-10 accelerometers mounted on the back end cylinder head. One accelerometer recorded vibrations along the cylinder's axis, while the other recorded movement in the transverse direction. Both accelerometers were connected to Unholtz-Dickie Mod D22 series charge amplifiers and data were recorded on a fifth Nicolet 4094 digital oscilloscope through 12 bit Type 4570 plug-ins, at a rate of 500,000 samples per second.

The physical vibration of the RCEM was thought to be a source of noise in the pressure and displacement data records as seen in Figure 5. This was confirmed by analyzing the vibration history of the machine.

Figure A.3 plots the transverse acceleration of the machine along with the position-time trace. It can be seen that the machine shakes considerably after the combustion event. This motion was concluded to be responsible for the jaggedness of the position data, and the sawtooth shape of the pressure record.

Exhaust Emissions - Due to the small quantity of combusted gas available, a series of steps were taken to maximize the analysis of the combustion products. After each run the cylinder gas was fed through an Omega Engineering, Inc. Model FMA 7305 flow controller and into the analyzer manifold. Separate

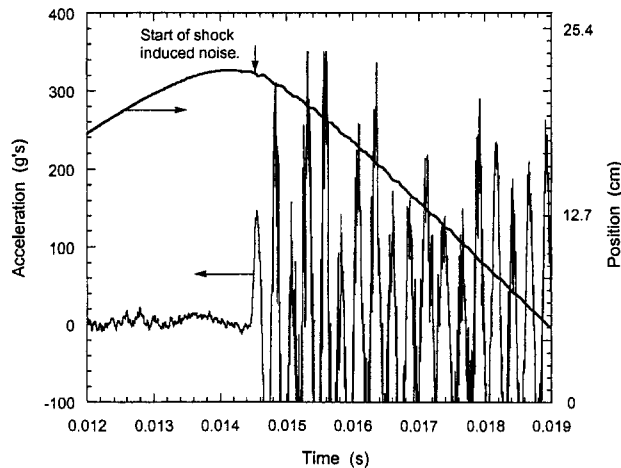


Figure A.3 - RCEM lateral acceleration and piston position vs. time.

valves were used to control the flow into each emissions analyzer. The feeds were split from the flow meter and only one analyzer used at a time. The free piston-cylinder arrangement maintained a constant back pressure on the combusted gases.

Analysis of the NO<sub>x</sub>, CO, CO<sub>2</sub>, and HC concentrations was achieved by alternating the flow through each emissions analyzer. The response time for each detector was quantified through the calibration procedure.

Emissions Calibration - Each of the analyzers used was calibrated in the same manner. First, appropriate zero and span gases from compressed gas cylinders were sent through each analyzer via the flow meter manifold described above. After each analyzer was calibrated, the span gas was reintroduced to the analyzer to determine the response time required to achieve consistent readings.

This procedure was then repeated, but this time with the zero and span gas sources located in the piston-cylinder device. The response time for data acquisition in this manner was also noted.

NO<sub>x</sub> Measurement - A Rosemont Analytical Model 951A NO<sub>x</sub> analyzer was employed for NO and NO<sub>x</sub> measurement. This analyzer was calibrated using a 6.7 parts per million (PPM) NO span gas. Since only one cylinder's worth of combustion products was available for analysis, the bypass flow was eliminated, and the burned gases pumped directly through the analyzer.

CO Measurement - A Rosemont Analytical Model 880A Non-Dispersive Infrared CO analyzer was employed for CO measurements. This analyzer was calibrated using an 801 PPM CO span gas.

CO<sub>2</sub> Measurement - A Rosemont Analytical Model 880A Non-Dispersive Infrared CO<sub>2</sub> analyzer was employed for CO<sub>2</sub> measurements. This analyzer was calibrated using a 3.89% CO span gas.

Unburned Hydrocarbon Measurement - A Rosemont Analytical Model 400A flame ionization hydrocarbon analyzer was employed for unburned HC measurements. This analyzer was calibrated using a 110 PPM propane-in-nitrogen background span gas. In this device the bypass flow was also eliminated, and the burned gases pumped directly through the analyzer.

Combustion Gas Analysis - In order to quantify leakage of the gases from the cylinder during the test sequence, the combusted

gases were periodically examined using pressure-volume-temperature (PVT) analysis. In this post test procedure the combustion products were expanded into a larger measurement tank (10 liters) to a pressure of approximately 80 Torr to ensure that all the water vaporized. Due to the small quantity of gas available only a PVT test or emissions analysis could be performed.

DISTRIBUTION:

1	MS 9108	E. Cull, 8414
1	9105	J. A. Lamph, 8118
1	9105	D. Zanini, 8118
1	9105	K. Pace, 8118
1	9105	S. Goldsborough, 8118
1	9105	N. Paradiso, 8118
1	9105	P. Van Blarigan, 8118
3	9018	Central technical Files, 8940-2(3)
1	0899	Technical Library, 4916
1	9021	Technical Communications Department, 8815/ Technical Library, MS 0899, 4916
1	9021	Technical Communications Department, 8815 For DOE/OSTI

Intentionally Left Blank